Effects of s~~S~~ea l~~L~~evel r~~R~~ise and t~~T~~idal f~~F~~lat g~~G~~rowth on t~~T~~idal d~~D~~ynamics and g~~G~~eometry of the Elbe e~~E~~stuary

Tara Franziska Mahavadi[1], Rita Seiffert[1], Jessica Kelln[1], Peter Fröhle[2]

[1]Federal Waterways Engineering and Research Institute, Hamburg, 22559, Germany
[2]Hamburg University of Technology, Hamburg, 21073, Germany

Correspondence to: Tara Mahavadi (tara.mahavadi@baw.de)

Abstract. Future global mean sea level rise (*SLR*), will affect coastlines and estuaries in the North Sea and therefore also coastal protection structures,~~as well as~~ ~~local~~ unique local ecosystems and important waterways. *SLR* will not only raise water levels~~,~~ but will also influence tidal dynamics~~-~~ and morphodynamics, which is why the tidal flats of the Wadden Sea can ~~potentially~~ grow to a certain extent with *SLR*. Investigations on the effects of climate change-~~-~~induced *SLR* and the related~~corresponding~~ potential bathymetric changes inside of estuaries form an important basis for identifying~~the identification of~~ vulnerabilities and developing~~the development of~~ appropriate adaptation strategies. ~~With the help of a highly resolved hydrodynamic-numerical model of the German Bight, we~~ To analyse the influence of potential *SLR* and tidal flat elevation scenarios on the tidal dynamics in the Elbe estuary, we used a highly resolved hydrodynamic-numerical model of the German Bight. The analysis results show increasing tidal range in the Elbe estuary solely due to *SLR*. They also reveal strongly varying changes with different tidal flat growth scenarios: while tidal flat elevation up to the mouth of the estuary can cause tidal range to decrease relative to *SLR* alone, tidal flat elevation in the entire estuary can lead to an increase in tidal range relative to *SLR* alone. ~~The results show an increase of tidal range in the Elbe estuary due to *SLR* and further reveal, that tidal flat growth can have no effect, decrease or increase the tidal range relative to sole *SLR*, depending on the location and amount of tidal flat elevation.~~ Further analyses show~~demonstrate,~~ how the geometric parameters of the Elbe estuary are changing due to *SLR* and tidal flat elevation. We discuss how these changes in estuarine geometry can provide~~be~~ an explanation for the changes in tidal range.

1 Introduction

Future global mean sea level rise (*SLR*)~~,~~ as it is projected for this century (Fox-Kemper et al., 2021)~~, will have a huge impact on coastal areas around the world. It~~ will not only raise water levels in the German Bight, but will also affect, for example, tidal dynamics (e.g. tidal amplitude and tidal asymmetry) in several ways (Jordan et al., 2021; Wachler et al., 2020). ~~-~~In particular, low-lying coastal areas such as the German Bight and the adjacent estuaries are vulnerable to changes due to *SLR*. ~~The German Bight, l~~Located in the North Sea, the German Bight includes a large part of the Wadden Sea World~~'s~~ Natural

Formatiert: Deutsch (Deutschland)
Formatiert: Deutsch (Deutschland)
Formatiert: Schriftart: Kursiv
Formatiert: Schriftart: Kursiv
Formatiert: Schriftart: Kursiv
Formatiert: Nicht unterstrichen, Schriftfarbe: Automatisch
Formatiert: Nicht unterstrichen, Schriftfarbe: Automatisch
Formatiert: Schriftfarbe: Automatisch
Formatiert: Nicht unterstrichen, Schriftfarbe: Automatisch
Formatiert: Nicht unterstrichen, Schriftfarbe: Automatisch

Heritage Site~~ Wadden Sea~~. The Wadden S~~s~~ea is a geologically and ecologically unique region, which is structured into several tidal basins with barrier islands, tidal channels and intertidal areas (Kloepper et al., 2017).

As a result of~~Due to~~ tidal flat morphodynamics (Friedrichs, 2011), ~~-~~ *SLR* will not only influence the tidal dynamics~~,~~ but also the bathymetry in the German Bight. Changes in tidal dynamics affect~~influence~~ net ~~-~~sediment transport and therefore bathymetry, which in turn influences tidal dynamics. As the ~~Due to the mutual interdependency between~~ hydrodynamic forces and the coastal profile are interdependent, they strive for a morphodynamic equilibrium ~~is striven towards~~ in theory (Friedrichs, 2011). Investigations show~~,~~ that in the recent past (1998-2016) most intertidal flats in the German Bight have been~~were~~ vertically growing at higher~~in a~~ rates ~~higher~~ than the observed mean *SLR* ~~sea level rise in the recent past (1998-2016)~~ (Benninghoff and Winter, 2019). However, in view of~~facing~~ the future acceleration of *SLR* *(Fox-Kemper et al., 2021)*, it is difficult to quantify ~~the amount~~ to what~~which~~ extent tidal flat growth can keep pace with~~-~~ *SLR*~~sea level rise~~, and it is~~remains~~ questionable, whether the present ~~-hydromorphodynamic~~ equilibrium between hydrodynamics and morphodynamis will be maintained in the future. Several studies found that tidal flats can potentially grow with *SLR*~~,~~ if sediment availability is sufficient, but cannot keep pace with ~~high~~ future high *SLR* scenarios (Becherer et al., 2018, van der Wegen, 2013, Dissanayake, 2012). A precise prediction of the future morphologic development of the Wadden Sea is difficult~~,~~ as it does not only depend on the rate of *SLR*~~,~~ but also on several other factors (~~as~~ e.g. vertical sediment structure, sediment availability and potentially changing meteorology). Furthermore, long-term numerical simulations of morphodynamic processes are challenging, because complex small-scale processes need to be parameterised and the spatial resolution of morphodynamic simulations is limited by computing power.

P~~In any case, p~~otential tidal flat growth should be considered when studying *SLR* ~~-~~scenarios, as it strongly affects the tidal dynamics in the Wadden Sea (Wachler et al., 2020; Jordan et al., 2021). *SLR* in the German Bight will cause an increase in tidal prism relative to channel cross-sectional ~~-~~flow area in the tidal basins and ~~therefore an increase of~~ current velocity in the channels will increase as a result. ~~,~~This effect ~~which~~ is counteracted by tidal flat elevation (Wachler et al., 2020). *SLR* can also cause a shift of the amphidromic point in the German Bight in eastward direction, which is ~~as well~~ counteracted by tidal flat elevation as well (Jordan et al., 2021). As a result of~~Due to~~ the changes in amphidromes and current velocities~~y~~, the combined effect of tidal flat elevation and~~with~~ *SLR* causes an increase in M2 ~~-~~amplitude in the German Bight relative to ~~sole~~ *SLR* alone (Jordan et al., 2021).

One of the main estuaries in the German Bight is the Elbe estuary (Figure 1), which contains the port of Hamburg and is therefore an important shipping route. The Elbe estuary is the part of the Elbe river that extends ~~extending~~ from the weir in Geesthacht to the North Sea (Figure 5). The weir in Geesthacht is the artificial tidal barrier of the estuary. ~~Further downstream, approximately where the estuary reunites again, after splitting into two branches, lies the port of Hamburg.~~ An artificially deepened fairway is maintained from the port of Hamburg to the North Sea~~,~~ to enable the passage of ~~allow~~ large container ships~~ to reach Hamburg~~. ~~The part of the estuary upstream of Hamburg to the town Brunsbüttel includes intertidal areas, the extent of which further increases upstream of Brunsbüttel in the dilating mouth of the estuary (Figure 5).~~ The Elbe estuary is

Formatiert: Nicht unterstrichen, Schriftfarbe: Automatisch

Formatiert: Nicht unterstrichen, Schriftfarbe: Automatisch

Formatiert: Schriftfarbe: Automatisch

Formatiert: Schriftart: Kursiv

Feldfunktion geändert

Formatiert: Schriftart: Kursiv

Formatiert: Schriftart: Nicht Kursiv

a strongly anthropogenically influenced system subject to strong anthropogenic influence (e.g. due to the containment by dikes and the deepening of the fairway deepening). While the tidal range in Cuxhaven, in the mouth of the estuary remained relatively constant at around 3 -m over the last 100 years, the tidal range in St. Pauli, close to the port of Hamburg increased over the last 100 years (Boehlich and Strotmann, 2019). Nowadays, the Elbe estuary is an amplified estuary, where the tidal amplitude increases in upstream direction and reaches its maximum close to the port of Hamburg. Further upstream, where the water depth decreases and river discharge becomes more relevant, the tide is damped and tidal amplitude decreases.

The future of the Elbe estuary depends not only on anthropogenic measures implemented on site, but also in particular on *SLR*sea level rise and its implications. *SLR* Sea level rise and (resulting) topographic changes will alter estuarine geometry and thus influence the tidal wave propagating into the estuary, which is generally modified by amplification, damping, reflection and distortion. The term "eEstuarine geometry" hereby denotes the form of the intersection of estuarine bathymetry with characteristic local parameters of the tide. *SLR* will not only simply raise water levels in estuaries; it can also cause changes in water level variations. Higher water levels can help deep-draught vessels navigate the estuary fairway, but at the same time can hinder the passage of ships beneath bridges due to reduced clearance. Changes in low tide levels can lead to difficulties in drainage into the estuary and can therefore impact agriculture in the hinterland, navigation in connected channels and tributaries, and urban drainage systems (Khojasteh et al., 2021). Moreover, changes in water level and variations of water levels (low tide and high tide levels) are relevant for the dimensioning of waterfront structures and other hydraulic structures in estuaries (HTG, 2020). In addition, changes in water level and tidal range can affect the inundation time of the intertidal area and can change the location and extension of the intertidal area. This in turn can impact biodiversity and agriculture. Other possible *SLR*-induced changes in tidal dynamics, besides an increase or decrease in tidal range, are changes in current velocities and tidal asymmetry and, therefore, e.g. enhanced flood dominance, which can result in more sediment import. A larger tidal range and stronger tidal asymmetry can cause fine sediments to be pumped into the estuary, which can reduce hydraulic drag. This can in turn led to an increase in tidal amplification eventually resulting in a hyper-turbid state (Winterwerp and Wang, 2013). Such developments in sediment dynamics can impact biodiversity and create economic challenges as a result of the siltation of navigation channels. Another possible consequence of *SLR* is increased saltwater intrusion into estuaries because of larger tidal prisms and water depths, with an effect on e.g. ecosystems, aquifers and agriculture (Khojasteh et al., 2021). Understanding the future evolution of tidal dynamics due to *SLR* in heavily utilized estuaries such as the Elbe estuary is therefore important for the development of adaptation measures, e.g. for navigation, port infrastructure and sediment management in the estuary, as well as water management in the hinterland.

Understanding the future evolution of tidal dynamics due to sea level rise in heavily utilised estuaries such as the Elbe estuary is important for the development of adaptation measures, e.g. in navigation, port infrastructure and water management.

Several model-based methods are available to address theseis questions. Analytical studies have examinedon the behaviour of tides in estuaries for have been conducted since many decades (Winterwerp and Wang, 2013). Several studies (e.g. (Jay, 1991;

Formatiert: Schriftart: Kursiv

Formatiert: Nicht unterstrichen, Schriftfarbe: Automatisch

Feldfunktion geändert

Formatiert: Nicht unterstrichen, Schriftfarbe: Automatisch

Formatiert: Schriftart: Kursiv

Formatiert: Nicht unterstrichen, Schriftfarbe: Automatisch

Formatiert: Nicht unterstrichen, Schriftfarbe: Automatisch

Feldfunktion geändert

Formatiert: Nicht unterstrichen, Schriftfarbe: Automatisch

Feldfunktion geändert

Feldfunktion geändert

Feldfunktion geändert

Friedrichs and Aubrey, 1994; Savenije et al., 2008; Friedrichs, 2010; van Rijn, 2011) developed, discussed and applied analytical solutions to estimate tidal wave propagation in estuaries by simplifying estuarine geometry and the basic equations. They ~~and~~ develop~~ing~~ed scaling parameters to describe the systems, while still including the important effects of intertidal area and channel convergence. In these analytical studies, simplified geometric properties of the studied estuaries are considered by the use of several characteristic parameters.

However, accurate computation of time-depended water levels and current velocities requires the application of advanced numerical models that are capable of~~, which can~~ considering various driving forces and their interactions with accurate concepts of energy exchange and a precise implementation of estuarine shape (Khojasteh et al., 2021). The importance of an accurate representation of the bathymetry ~~in numerical models~~ of shallow coastal systems in numerical models~~,~~ is pointed out by Holleman and Stacey (2014) and Rasquin et al. (2020). Rasquin et al. (2020) found that insufficient bathymetric resolution may lead to overestimation of the tidal amplitude increase in the German Bight~~find, that the increase of tidal amplitude in the German Bight due to *SLR* can be overestimated, if bathymetric resolution in the model is insufficient~~. A study by Seiffert and Hesser (2014) investigating the effect of *SLR* on the tidal dynamics in the Elbe estuary shows~~,~~ that *SLR* causes ~~an increase of~~ the tidal range in the Elbe estuary to increase. However, this study does not consider the potential vertical growth of tidal flats with *SLR*. Even if the future morphologic development of the tidal flats in the German Bight and the Elbe estuary is difficult to predict, potential topographic changes might have a considerable impact on tidal dynamics and should not be neglected.

A drawback~~ownside~~ of advanced numerical models, besides the computational time and resources required, is the loss of simplicity, and hence transparency. Therefore, extensive analysis of the simulation results is necessary to gain ~~a~~ system understanding and ~~to~~ provide an insight ~~on~~ how certain parameters affect others. For this purpose, it can be useful to analyse simplified geometric parameters, which were originally developed in the context of analytical estuary models.

In this study, potential future *SLR* and tidal flat growth scenarios are simulated using a hydrodynamic-numerical model. The two issues we want to address in this study are the following: 1. What is the influence of potential future *SLR* and tidal flat growth scenarios on the tidal range along the Elbe estuary? 2. How can these changes be explained by changes in estuarine geometry? The general aim of this study is to gain a better understanding of the possible effects of potential *SLR* and tidal flat growth scenarios in the Elbe estuary.

Tidal range is the double of tidal amplitude and the difference between tidal high water and tidal low water. It is an integral part of the energy flux of a propagating tidal wave. As mentioned before, it is a parameter that has an influence on navigation in the estuary and drainage into the estuary, as well as on the dimensioning of bank structures. Moreover, the tidal range in an estuariy is closely linked with tidal current velocity, mixing, circulation, sediment transport, water quality and ecosystem communities (Khojasteh et al., 2021). We therefore focus on this parameter as it is a highly reliable result of hydrodynamic numerical simulations compared to other parameters mentioned.

~~Our objective is to investigate how tidal range along the Elbe estuary is influenced by potential future *SLR* and tidal flat growth scenarios. Tidal range is the double of tidal amplitude and the difference between tidal high water and tidal low water. It is an~~

Feldfunktion geändert

Feldfunktion geändert

Feldfunktion geändert

Formatiert: Schriftart: Kursiv

Formatiert: Schriftart: Kursiv

Formatiert: Schriftart: Kursiv

Feldfunktion geändert

Formatiert: Deutsch (Deutschland)

~~integral part of the energy flux of a propagating tidal wave. Tidal range in estuaries is closely linked with tidal current velocity, mixing, circulation, sediment transport, water quality and ecosystem communities~~ (Khojasteh et al., 2021)~~. Additionally, it is a parameter which has an influence on navigation in and drainage into the estuary, as well as on the dimensioning of waterfront structures and other hydraulic structures in the estuary~~ HTG (2020)~~.~~

Feldfunktion geändert

Formatiert: Deutsch (Deutschland)

Feldfunktion geändert

To find explanatory approaches for the changes in tidal range simulated by our hydrodynamic-numerical model, we analyse three parameters of estuarine geometry (mean hydraulic depth, convergence of cross-sectional flow area and relative intertidal area). These geometric parameters, which describe the shape of the estuary in a simplified way, are (equally or in similar form) known from previously mentioned analytical models.~~ We investigate not only the effect of sole *SLR* scenarios, but also a bandwidth of corresponding simplified hypothetical tidal flat growth scenarios. In our study scenarios of potential future sea level rise and tidal flat growth scenarios are simulated using the three-dimensional hydrodynamic-numerical method UnTRIM² (Casulli, 2009) in a regional model of the German Bight, to access the influence on tidal range in the Elbe estuary. The aim of this study is to gain a better understanding of the possible effects of potential *SLR* and tidal flat growth scenarios in the Elbe estuary. In addition to characteristic parameters of the vertical tide, we analyse three parameters of estuarine geometry (mean hydraulic depth, convergence of cross-sectional flow area and relative intertidal area). These geometric parameters, which describe the shape of the estuary in a simplified way, are (equally or in similar form) known from previously mentioned analytical models and are herein used to find explanatory approaches for the changes of tidal dynamics simulated by the advanced hydrodynamic-numerical model.~~

Formatiert: Hervorheben

T~~In t~~he subsequent Sect.~~chapter~~ 2 describes the applied methods~~ will be described~~. It includes a short description of the model and the simulated scenarios. T~~Moreover, t~~he analysed geometric parameters of the estuary and their potential influence on tidal range are shortly discussed in this section. In Sect.~~chapter~~ 3 the results of the analysed tidal and geometric parameters for some of the examined scenarios are illustrated ~~displayed~~ and outlined. The ~~Chapter 4 includes a discussion on the~~ possible reasons for the detected changes in estuarine geometry and~~, as well as~~ the potential role of a changing geometry in the alteration of tidal range in the estuary are discussed in Sect. 4.~~.~~ Finally, Sect.~~chapter~~ 5 summarises the main findings of this study and their relevance and suggests questions that should be investigated in ~~gives an outlook on open questions for~~ future studies~~investigations~~.

2 Theory and m~~M~~ethods

2.1 Model setup

For this study the three-dimensional hydrodynamic numerical model UnTRIM² (Casulli, 2009) is used, which solves the three-dimensional-shallow water equations and the three-dimensional transport equation for e.g. salt, suspended sediment and heat on an orthogonal unstructured grid (Casulli and Walters, 2000). A special feature of UnTRIM² compared to its predecessor UnTRIM is the subgrid technology, which allows a high resolution of the topography independently of the computational grid

(Casulli, 2009). The computational grid cells can be wet, partially wet, or dry, allowing a precise mass balance and~~ a~~ realistic wetting and drying (Sehili et al., 2014), which is important for a realistic representation of the large intertidal areas in the German Bight. The variation of the surface drag coefficient with wind speed is parametrised according to ~~S. D.~~ Smith and~~ E. G.~~ Banke (1975). The generation of wind waves as well as sediment and heat transport are not calculated in the model setup used for this study in order to reduce computational effort.

The regional model we use is very similar to the model used by Rasquin et al. (2020). The model domain covers the German Bight from Terschelling in the Netherlands to Hvide Sande in Denmark including the estuaries of the Elbe, Weser and Ems rivers with their main tributaries (Figure 1). The model boundary is defined by the dike line and thus~~ which therefore~~ cannot be overflowed. The resolution of the computational grid ranges from ~~varies between ~~5 km at the open boundary to about 100 m in the coastal area and the estuaries. In ~~A higher subgrid resolution is used in ~~the Wadden S~~s~~ea region and the estuaries a higher subgrid resolution of about 10 m to 50 m in the finest part is used. The model has vertically fixed layers with ~~Throughout the model domain, the vertical ~~ a grid resolution of~~is~~ 1 m up to a depth of 27.5 m and a resolution of 10 m below this depth~~that~~. The topography data of the year 2010 implemented into the model were~~as~~ generated in the EasyGSH-DB project (Sievers et al., 2020).

The atmospheric forcing over the model domain (wind field at 10 m height and surface pressure) is derived from COSMO-REA6 (Bollmeyer et al., 2015). The data are~~is~~ generated and made available by the Hans Ertel Centre~~er~~ of the University of Bonn in cooperation with~~ the~~ Germany's National Meteorological~~Weather~~ Service (Deutscher Wetterdienst, DWD) (Bollmeyer et al., 2015). Salinity is set to a constant value of 33 psu~~PSU~~ at the open boundary (based on BSH (2016)) and 0.4 psu~~PSU~~ (based on Bergemann (2009)) at the upstream boundary of the Elbe estuary.

The German Bight model is used to simulate a~~A~~ spring–neap cycle in July 2013 with a constant river discharge at the upstream boundary of the Elbe estuary of 600 m³/s~~ is simulated with the German Bight model~~. The weir in Geesthacht is open~~laid~~ in the model during the simulated period. The selected period and discharge are chosen to estimate changes in~~of~~ average conditions without extreme events. ~~Sea level rise is added at the open boundary of the German Bight Model.~~

Water levels at the seaward open boundary of the German Bight model are~~is~~ provided by the Dutch continental shelf model (DCSMv6FM) (Zijl, 2014), a 2-D hydrodynamic~~al~~ model which covers the north-western European shelf and which is a further development of DCSMv6 (Zijl et al., 2013; Zijl et al., 2015) (Figure 1). DCSMv6FM uses~~is using~~ the flexible mesh technique D-Flow FM (DFlow Flexible Mesh) (Kernkamp et al., 2011)~~, which is ~~based on the classical unstructured grid concept. At the seaward open boundary, the DCSMv6FM model is forced by the amplitudes and phases of the 22 main diurnal and semidiurnal constituents, which are derived by interpolation from the data set generated by the GOT00.2 global ocean tide model (Ray, 1999). Sixteen additional partial tides are adopted from FES2012 (Carrère et al., 2013). As for the smaller regional model, the atmospheric forcing for DCSMv6FM is derived from COSMO-REA6 (Hans-Ertel-Centre for Weather Research; (Bollmeyer et al., 2015).

SLR is added at the open boundary of the German Bight Model, therefore *SLR*-induced changes in tidal dynamics seaward of the German Bight are neglected. Ideally, *SLR* would be added at the boundary of the shelf model to consider changes in tidal

Feldfunktion geändert

Feldfunktion geändert

Feldfunktion geändert

Feldfunktion geändert

Formatiert: Schriftart: Nicht Kursiv

Formatiert: Schriftart: Nicht Kursiv

Formatiert: Schriftart: Nicht Kursiv

Formatiert: Schriftart: Nicht Kursiv

Formatiert: Schriftart: Nicht Kursiv

Formatiert: Schriftart: Nicht Kursiv

Formatiert: Schriftart: Nicht Kursiv

Formatiert: Schriftart: Kursiv

dynamics in the continental shelf seaward of the German Bight Model boundary. However, this approach is not suitable in our case, since the resolution of the DCSMv6FM is insufficient for estimating *SLR* induced changes (Rasquin et al., 2020).

Formatiert: Schriftart: Nicht Kursiv

Formatiert: Schriftart: Kursiv

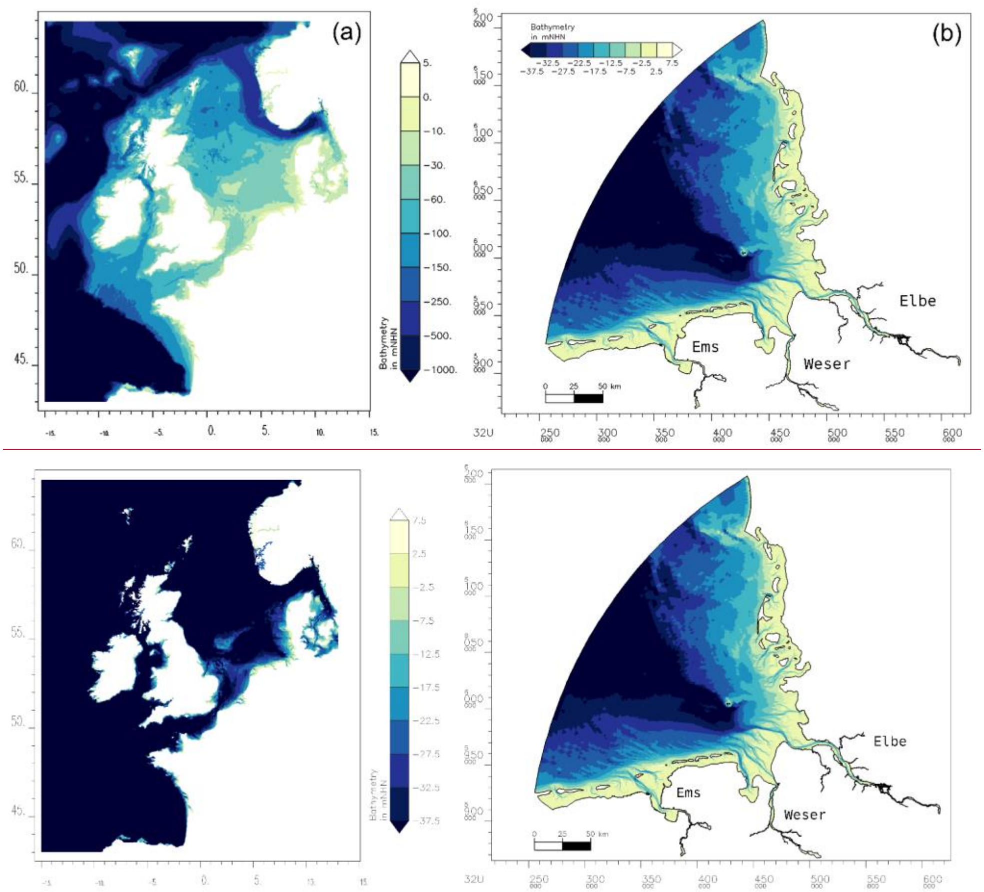

Figure 1: Model domain and bathymetry in m NHN (German vertical datum) of the *DCSMv6FM* model (a~~left~~) in WGS 84 and of the German Bight model (b~~right~~) in UTM zone 32N.

Since the focus of our study is on the Elbe estuary, a brief validation of the model for~~in~~ this specific region is presented below. Further analysis of the~~n~~ model's performance can be found in Rasquin et al. (2020). To compare the simulation results with observations, we simulated seven spring-neap-cycles between January and April 2013 with measured river discharge provided by the Federal Waterways and Shipping Agency (WSV, 2022). A comparison of water levels between model results and observations at 39 gauges in the model domain for this period reveals a mean RMSE of 16.4 cm, a mean bias of 7.3 cm and a mean skill score after Willmott et al. (1985) of 0.993. Figure 2 shows a visual comparison between the simulation result and the observation of the water level at the stations of Cuxhaven (mouth of the estuary) and St. Pauli (close to the port of Hamburg) for a short period of time. It can be seen that the phase and shape of the vertical tide are~~is~~ well reproduced by the model, but tidal low water is slightly higher in the simulation results compared to the observations. A similar display for an entire spring–neap cycle can be found in the appendix. It shows that there are no distinctive differences in performance during the different phases of the illustrated spring–neap cycle.

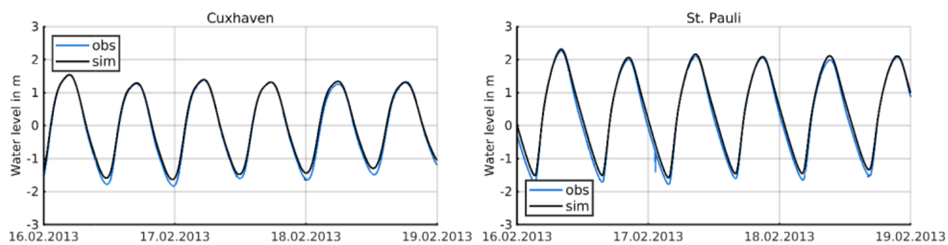

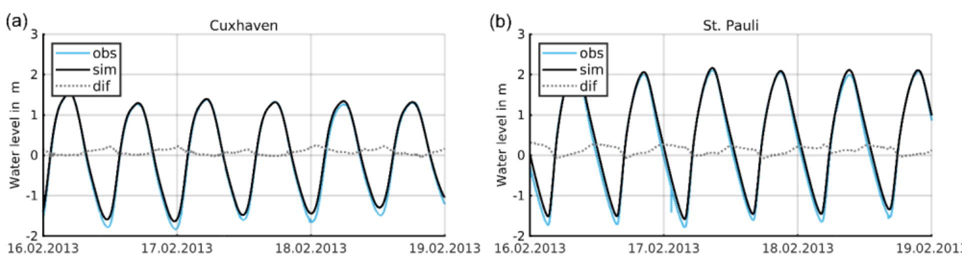

Figure 2: Simulated ~~Water level from simulation result~~ (black) and observed~~ation~~ (blue) water levels and the difference between simulation and observation (gray) at the stations in Cuxhaven (a) and St. Pauli (b)

Figure 3 shows the mean tidal range (*TR*) and mean tidal mean water level (*MW*) along the estuary for the seven spring–~~-~~neap ~~-~~cycles, calculated for both the simulation results and observational data at stations along the estuary (WSV, 2022). It demonstrates~~shows~~, that the model is able to reproduce the characteristic development of *TR* along the Elbe estuary, with a strong increase starting at around km -60, a maximum reached around km -115 and a decrease further upstream. As a result of the too high tidal low water, the model underestimates *TR* ~~is underestimated~~ by 10–~~-~~20 -cm and overestimates *MW* ~~water is overestimated by the model~~ by around 10 -cm. The *RMSE* for the mean *TR*, *MW*, tidal high water *(HW)* and tidal low water *(LW)* for the gauges Cuxhaven, St. Pauli and the mean of 15 gauges in the Elbe estuary is shown in Table 1.

Feldfunktion geändert

Feldfunktion geändert

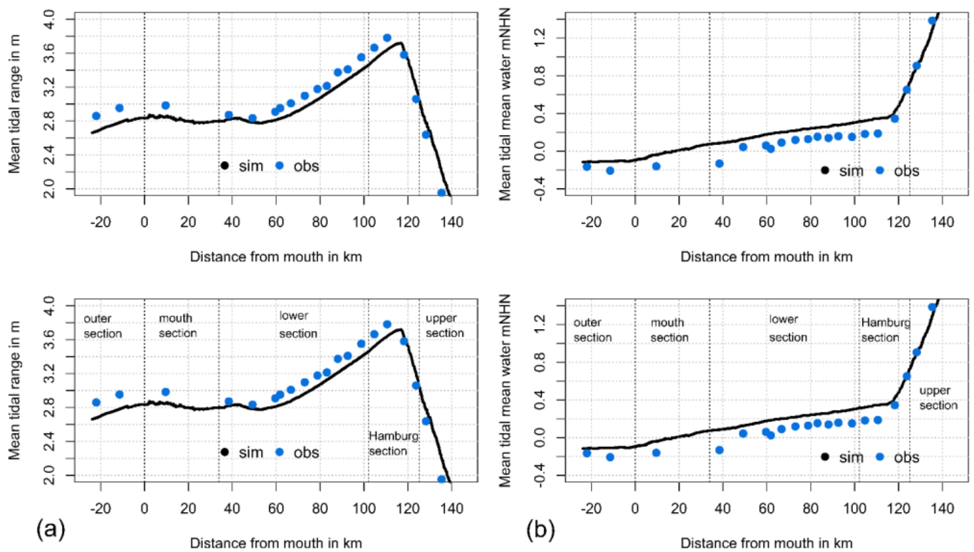

Figure 3: *TR* (~~a~~left) and *MW* (~~b~~right) above mNHN (mete~~rs~~res above the German datum) averaged over 7 spring–neap-cycles from ~~in~~ January 2013 to April 2013 along the Elbe estuary, calculated from observations (blue) and from ~~the~~ simulation results (black).

Formatiert: Schriftart: Kursiv

Formatiert: Schriftart: Kursiv

Table 1: Root-mean-square error for tidal parameters of water level in the Elbe estuary

Formatierte Tabelle

Location	*RMSE of TR*	*RMSE of HW*	*RMSE of LW*	*RMSE of MW*
Cuxhaven	15.7 cm	11.4 cm	21.4 cm	13.2 cm
St. Pauli	17.2 cm	12.9 cm	23.6 cm	17.3 cm
Mean of gauges in the estuary	16.8 cm	11.7 cm	20.9 cm	13.7 cm

2.2 Simulated ~~s~~Scenarios

To investigate the effect of *SLR* and potential corresponding tidal flat growth, several scenarios are simulated and analysed. Two *SLR* -scenarios of 55 cm and 110 -cm were simulated by adding *SLR* at the open boundary of the German Bight model. According to the IPCC 6th Assessment Report (AR6), mean global *SLR* in 2100 compared to the reference period 1995–2014 will be in the~~a~~ likely range between ~~of~~ 0.43 m and ~~to~~ 1.01 -m for the intermediate- to high-emission -scenarios (SSP2-4.5, SSP3-7.0 and SSP5-8.5) (Fox-Kemper et al., 2021). Our selected *SLR* -scenarios are close to the median of the intermediate scenario and close to the upper range of the high-emission scenario for 2100. Projected values for regional *SLR* in the southeastern North Ssea region (Delfzijl, Cuxhaven, Esbjerg) are within a range of ±20 cm of the median of the projected global mean *SLR* until 2100 (Fox-Kemper et al., 2021; Garner et al., 2021).

As mentioned in the introduction, there are uncertainties and difficulties in quantifying to what extent theit is uncertain and difficult to quantify to which amount tidal flats in the German Bight will be able to keep up with future accelerated *SLR*. The amount of tidal flat accretion can strongly differ between the tidal basins of the German Bight and doesis not only dependent on future *SLR* acceleration and magnitude, but also on sediment availability and meteorological conditions. To gain a better understanding of the possible effects of potential *SLR* and tidal flat growth scenarios in the Elbe estuary, we analyse a range of 0 %, 50 % and 100 % tidal flat growth with *SLR*. In these scenarios, all tidal flat areas in the entire model domain are uniformly elevated by the samea certain amount, which is a highly simplified assumption.

Formatiert: Standard

Table 21: Simulated scenarios

Sscenario	SLR	Tidal flat elevation
ref	-	-
slr55t0	+55 cm	-
slr55tf55a	+55 cm	+55 cm Scenario A
slr55tf55be	+55 cm	+55 cm Scenario B
slr110t0	+110 cm	-
slr110tf55a	+110 cm	+55 cm Scenario A
slr110tf110a	+110 cm	+110 cm Scenario A
slr110tf55be	+110 cm	+55 cm Scenario B
slr110tf110be	+110 cm	+110 cm Scenario B

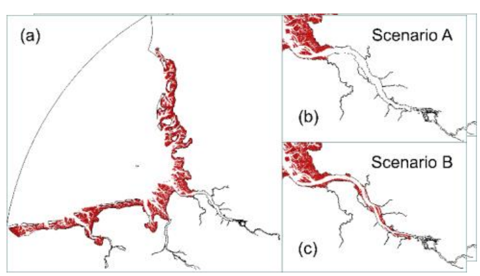

Figure 4: Areas of tidal flat elevation in the model domain (a) and in the Elbe estuary for two different scenarios (b) and (c)

The scenarios with tidal flat growth are further differentiated by firstly by elevating the tidal flats in the German Bight and in the mouth section of the Elbe estuary (Sscenario A) and secondly by elevating the tidal flats in the German Bight, the mouth

Formatiert: Standard

section and also the lower section of the estuary (S~~s~~cenario B) (see Figure 4). The purpose of this~~This~~ differentiation inside the estuary is~~ done~~ to gain a better understanding of the estuarine system in the context of *SLR* and tidal flat elevation. Table 2~~Table 1~~ summarises the scenarios simulated with the German Bight model. The letters ‘a’ and ‘b’ in the names stand for Scenarios A and B, while ‘tf’ stands for ‘tidal flats’.~~.~~

2.3 Analysis of s~~S~~imulation r~~R~~esults

2.3.1 Spatial d~~D~~ecomposition and d~~D~~efinition

Our study area is the Elbe estuary, i.e. the tidally influenced part of the river Elbe that extends from the weir in Geesthacht to the North Sea (Figure 5). The weir in Geesthacht is the artificial tidal barrier of the estuary. The estuary splits into two branches that reunite close to the port of Hamburg (Figure 5). To enable the passage of large container ships travelling to Hamburg, an artificially deepened fairway is maintained up to the port. The part of the estuary between Hamburg and the city of Brunsbüttel includes intertidal areas, and several islands and is connected to a number of small tributaries (Figure 5). The widening mouth of the estuary with its large intertidal areas interfused by several smaller and larger channels is located between Brunsbüttel and Cuxhaven. Mean tidal parameters are analysed and visualised along the profile of the estuary. The profile is displayed in Figure 5;~~,~~ it starts seaward~~s~~ of the mouth of the estuary and runs upstream along the fairway~~,~~ and ~~along~~ the northern branch up to~~until~~ the weir in Geesthacht. For the analysis of the geometric parameters, the estuary is divided into 71 control volumes (Figure 5). As the Elbe estuary splits into two branches, which reunite close to the port of Hamburg and enclose the island of Wilhelmsburg, this region is contained in one relatively large control volume compared to the other control volumes. The control volumes and consequently,~~therefore~~ the analysed geometric parameters do not cover the full length of the estuary profile, as a clear definition of the boundaries is not possible in the outer section of the estuary. However, the tidal parameters are analysed and displayed along the entire profile, even in the outer section. For a better comparison between the tidal parameters along the profile and the geometric parameters derived for the control volumes, the zero position of the x-axis in the figures showing the results along the estuary is set at the most seaward control volume boundary of the profile. Furthermore, the estuary is roughly divided into five sections, which are shown~~displayed~~ in Figure 5 and referred to~~named~~ (from west to east)~~:~~ as outer section, mouth section, lower section, Hamburg section and upper section.

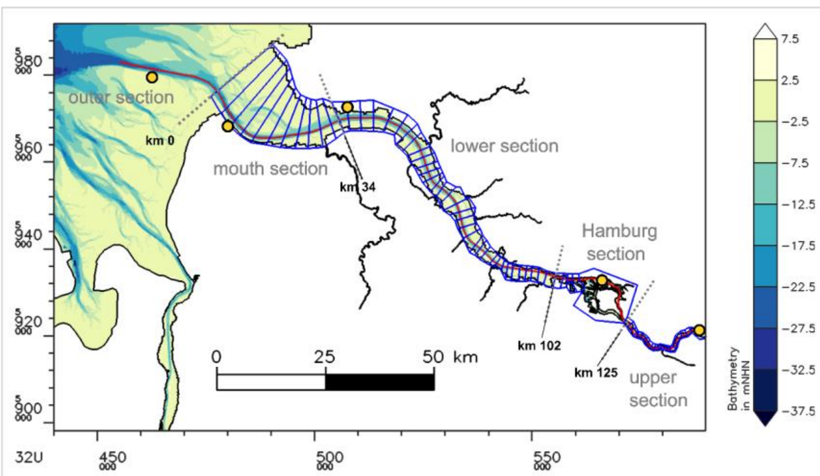

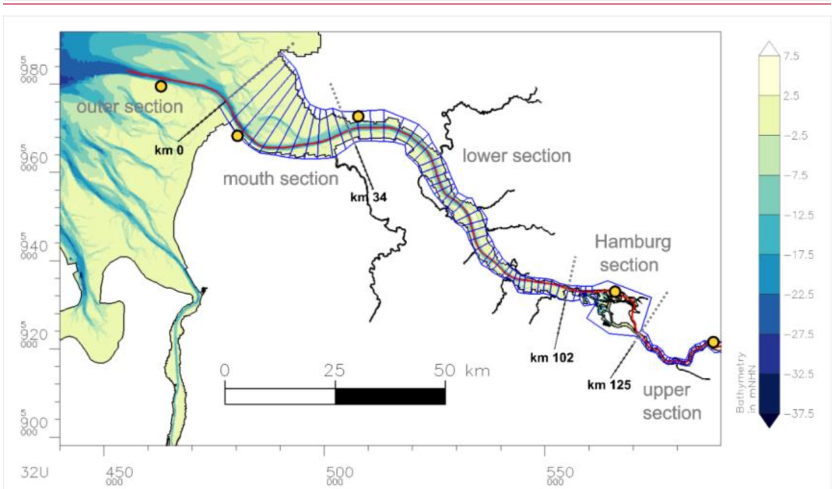

Figure 5: Model excerpt of the Elbe estuary showing ~~with a display of~~ the profile along the estuary (red) and a subdivision into 5 sections (grey) and 71 control volumes (blue) that~~which~~ are used for the analysis of the simulation results. The yellow markers represent the following locations from left to right: Scharhörn, Cuxhaven, Brunsbüttel, St. Pauli (Hamburg Port~~Harbour~~) and Geesthacht

2.3.2 Tidal and geometric p~~P~~arameters

The results of the hydrodynamic-numerical simulation are analysed by calculating the characteristic parameters of the vertical tide for the domain of the Elbe estuary. Further details about the method of the applied tidal analysis can be found in Lang (2003) and BAW (2017). All parameters are analysed for one spring–~~-~~neap cycle in July 2013, simulated with a constant discharge of 600 m³/s. The m~~M~~ean tidal parameters of the spring–~~-~~neap cycle are analysed and visualised along the profile of the estuary shown ~~displayed~~ in Figure 5. This study mainly focuses on the changes in mean tidal range (*TR*). *TR* is a key~~central~~ parameter in the estuary for characteriz~~s~~ing tidal dynamics, as it is closely linked to other tidal parameters (e.g. low water (*LW*), high water (*HW*)) which are relevant for navigation, drainage into the estuary and dimensioning of hydraulic structures. To derive explanatory approaches for the changes in~~of~~ *TR*, the changes in the~~of~~ estuarine geometry are analysed. The geometric parameters are obtained~~derived~~ by analysing the values for the 71 control volumes/areas along the estuary shown ~~which are displayed~~ in Figure 5. In the following section, the three geometric parameters studied will be introduced: convergence length (L_a), mean hydraulic depth (h) and relative intertidal area (φS_{INT}). The ~~geometry of an estuary influences~~ tidal dynamics in an estuary are influenced by its geometry in several ways. As our focus is on *TR*, we shortly discuss the potential influence of these three geometric parameters on *TR* in an estuary.

2.3.3 Convergence l~~L~~ength

Background

Upstream convergence of an estuary can cause upstream amplification of tidal waves. This phenomenon is also known~~denoted~~ as “~~‘~~wave shoaling”~~’~~ or “~~‘~~wave funnelling”~~’~~ (van Rijn, 2011). The tidal wave amplification due to the gradual change in the~~of~~ width and depth ~~-~~of a system can be explained with the wave energy flux equation~~,~~ as described ~~it is done~~ in Green's Law 1837 (van Rijn, 2011):

Eq. (1):

$$F = 0.125\rho g b H^2 c = Ec, \qquad (1)$$

w~~W~~here *F* is the energy flux per unit time (wave period) of a progressive sinusoidal wave being equal to *E* the energy of the wave per unit length of the wave times $c=(gh)^{0.5}$ the wave propagation celerity in shallow water. ~~With~~ *H* is~~being~~ the tidal wave height (tidal range), *b* is the width of the channel, *h* is the water depth, *ρ* is the water density and *g* is the gravitational acceleration. According to Green's Law, when the tidal wave is assumed to be a progressive sinusoidal wave in a system without reflection and energy loss due to friction, energy flux is constant and it follows that tidal amplitude varies as $b^{-1/2} h^{-1/4}$ with the channel width (*b*) of the momentum conveying–~~-~~stream and the depth (*h*) below ~~a~~ mean tidal water level (Jay, 1991). In an estuary containing a channel and tidal flats, the amplitude varies as $b^{-1/4} b_T^{-1/4} h^{-1/4}$ where~~ith~~ b_T is~~being~~ the width at mean water level (Jay, 1991). Based on these considerations, a gradual upstream decrease in the~~of~~ cross-sectional ~~-~~flow area *A* (*A*=*hb*) can cause an increase in tidal amplitude and therefore *TR*, and an increase of *A* can cause a decrease in~~of~~ *TR* accordingly.

Feldfunktion geändert

Feldfunktion geändert

Feldfunktion geändert

Feldfunktion geändert

Feldfunktion geändert

Feldfunktion geändert

Formatiert: Schriftart: Nicht Kursiv

Formatiert: Schriftart: Nicht Kursiv

Formatiert: Schriftart: Nicht Kursiv

Analysis of convergence length

A funnel~~-~~shaped geometry with decreasing width and depth in upstream direction is typical of~~for~~ most alluvial estuaries (van Rijn, 2011). A schematic plan view of a funnel~~-~~shaped estuary is shown in Figure 6. A mathematical way to represent the shape of an estuary, which has been~~ widely~~ used in many studies (Gisen, 2015), is an exponential function in the form of:

Eq. (2):

$$A = A_0 e^{-\frac{x}{L_a}}, \qquad (2)$$

w~~W~~here A is the cross-sectional-area, A_0 is the cross-sectional area at x=0 (mouth of the estuary), x is the distance from the mouth of the estuary in upstream direction along the estuary axis and L_{a} is defined as convergence length (the distance from the mouth at which the tangent through the point (0, A_0) intersects with the x-axis) (Savenije, 2012). The parameter L_{a} describes the rate of the decrease in the~~of~~ cross-sectional area in upstream direction. When comparing the convergence length between different estuaries or between different scenarios of the same estuary, a smaller value of L_{a} indicates a stronger convergence. It should be noted~~,~~ that some studies use the convergence length based on~~of~~ width, and sometimes depth, instead of the convergence length of cross-sectional ~~-~~area (A), to describe the shape of an estuary. Furthermore, several studies ~~do not~~ calculate more than~~only~~ one convergence length for an entire estuary~~, but~~ by dividinge it ~~estuaries~~ into sections with distinct convergence lengths.

However, we calculate only one convergence length (L_{a}) for the entire estuary to analyse possible changes in~~of~~ convergence for the entire system. We analyse L_{a} for each simulated scenario by fitting the exponential function of Eq. (2) to the data of the mean cross-sectional ~~-~~flow ~~-~~area at the control volume boundaries along the estuary, which are derived by analysings ~~of~~ the simulation results. The mean cross-sectional ~~-~~flow ~~-~~area is derived by averaging the mean cross-sectional ~~-~~flow ~~-~~area of each tide over the spring~~–~~neap ~~-~~cycle. The exponential function is fitted with a weighted multiple non-linear ~~-~~least-square regression using the G~~g~~auss-N~~n~~ewton-algorithm. The regression is performed with the nls-toolbox of the R-project (Baty et al., 2015). A multiple regression is necessary to analyse~~,~~ whether the convergence lengths of the different scenarios are significantly differing. A weighted regression is conducted to reduce the effect of uneven data distribution along the x-axis due to unevenly sized control volumes.

2.3.4 Mean hydraulic d~~D~~epth

Background

Water depth influences the propagation speed of a tidal wave c in shallow water in the form of $c=(gh)^{0.5}$. According to the wave energy flux equation mentioned above (Eq. (1)), an increase in water depth can therefore increase wave propagation speed and diminish~~ecrease~~ TR, if all other parameters remain constant. However, this would be a simplified assumption~~,~~ as it excludes bottom friction and other shallow water effects which become increasingly important closer to the coast where~~, when~~ the ratio of tidal amplitude (a) to ~~is less small than~~ water depth (h) increases. Energy dissipation due to work done by bed shear stress causes damping of the wave (decrease in~~of~~ TR). The w~~W~~ater depth in an estuary therefore affects the frictional damping

Feldfunktion geändert

Formatiert: Schriftart: Nicht Kursiv

Formatiert: Schriftart: Nicht Kursiv

of a tidal wave due to energy dissipation which scales by the cube of current velocity over depth (U^3/h) (Simpson and Hunter, 1974; Garrett et al., 1978). Therefore, a greater~~increased~~ mean water depth in the estuary can have the~~an increasing~~ effect of increasing ~~on~~ *TR* by reducing frictional damping of the tidal wave and vice versa. Furthermore, a change in mean water depth can also lead to a change in~~change~~ *TR* by pushing the system closer to or away from resonance (Talke and Jay, 2020).

Feldfunktion geändert

Analysis of mean hydraulic depth

The depth over an estuary cross-section (~~see~~ Figure 6) can be highly variable due to deep channels and shallow intertidal areas. The mM~~M~~ean hydraulic depth of an estuary can be defined and calculated in several ways (Zhou et al., 2018).~~, as discussed by Zhou et al. (2018).~~ Many studies with simplified models assume that~~only~~ the~~ channel as~~ flow-conveying cross-section solely comprises the channel, excluding the intertidal area. M~~Therefore, m~~ean hydraulic depth can thus be defined either including or excluding the intertidal area, which has a strong influence on the resulting ~~-~~value~~mean hydraulic depth~~. Two different definitions, one including intertidal area in the calculation of mean hydraulic depth ~~which include~~ (h_t) and the other excluding it from the calculation~~e~~ (h_c), ~~intertidal area into the calculation of mean hydraulic depth~~ are:

Feldfunktion geändert

Eq. (3):

$$h_\mathrm{t} = \frac{V_{MW}}{S_{MW}}, \quad (3)$$

and

Eq. (4):

$$h_\mathrm{c} = \frac{V_\mathrm{LW}}{S_\mathrm{LW}} + (MW - LW), \quad (4)$$

Where~~ith~~ V_MW, S_MW, V_LW and S_LW are~~being~~ the volume (*V*) and the surface area (*S*) at mean water level (*MW*) and mean low water level (*LW*), respectively (see Figure 6)). We calculate the mean hydraulic depth in each control volume and section for each scenario by using the volume and wetted surface area of the control volumes from the simulation results. Mean hydraulic depth is calculated according to Eq. (3) for the entire cross-section (h_t) and according to Eq. (4) for the channel part of the cross-section only (h_c). The mean volume (*V*) and wetted surface area (*S*) at *MW* and *LW* are~~is~~ derived by averaging over the spring ~~-~~neap ~~-~~cycle.

Formatiert: Schriftart: Nicht Kursiv

Formatiert: Schriftart: Nicht Kursiv

Formatiert: Schriftart: Nicht Kursiv

Formatiert: Schriftart: Nicht Kursiv

2.3.5 Relative intertidal a~~A~~rea

Background

The i~~I~~ntertidal area is approximately the area of the tidal flats~~,~~ between tidal low water (*LW*) and tidal high water (*HW*), which is subject to ~~periodically~~ wetting and drying cycles. Along-estuary transport of mass and momentum over tidal flats is often assumed to be negligible (Friedrichs, 2010). Tidal flats mainly store water instead of transporting momentum along the estuary (Aubrey and Speer, 1985). Momentum is lost as water flows onto the tidal flats with rising tide and decelerates because of strong friction, and also with~~at the~~ falling tide, as water with zero momentum returns to the momentum carrying channel and must be accelerated (Jay, 1991). Therefore, a loss of intertidal area causes an increase in tidal amplitudes and an enlargement~~increase~~ of intertidal area causes a decrease in tidal amplitude (Jay, 1991). According to Song et al. (2013), tidal flats a~~e~~ffect the tidal energy budget by storage and dissipation, while the former can be more significant than the latter. This means that ~~Based on these considerations~~ an increase in~~of~~ the relative~~.~~ intertidal area (ϙS_{INT}) can cause a decrease in~~of~~ *TR* and vice versa.

Analysis of the relative intertidal area

A tidal basin or an estuary can be roughly divided into a subtidal (S_{LW}) and an intertidal area (S_{INT}) (Figure 6). The i~~I~~ntertidal area (S_{INT}) is ~~hereby~~ defined as the difference between wetted surface area at mean high water and wetted surface area at mean low water:

Formatiert: Schriftart: Nicht Kursiv

Eq. (5):

$$S_{\mathrm{INT}} = S_{\mathrm{HW}} - S_{\mathrm{LW}}, \qquad (5)$$

The r~~R~~elative intertidal area (ϙS_{LW}) can be defined as the ratio between S_{INT} and S_{HW}:

Formatiert: Schriftart: Nicht Kursiv

Formatiert: Schriftart: Nicht Kursiv

Formatiert: Schriftart: Nicht Kursiv

Eq. (6):

$$ϙS_{\mathrm{INT}} = \frac{S_{\mathrm{INT}}}{S_{\mathrm{HW}}} = \frac{S_{\mathrm{HW}} - S_{\mathrm{LW}}}{S_{\mathrm{HW}}}, \qquad (6)$$

Different ratios are commonly used to describe the cross-sectional geometry and can~~ be~~ often be converted into each other. They ~~and~~ are ~~in detail~~ discussed in detail by Zhou et al. (2018). We define relative intertidal area as the ratio of~~between~~ intertidal area to~~and~~ wet surface area at mean high water (ϙS_{INT}) (Eq. (6)). According to Eq. (6), we calculate the relative intertidal area for each control volume and section for each scenario. The m~~M~~ean wetted surface area at *HW* and *LW* is derived from the simulation results for each control volume and averaged over the spring~~-~~neap ~~-~~cycle.

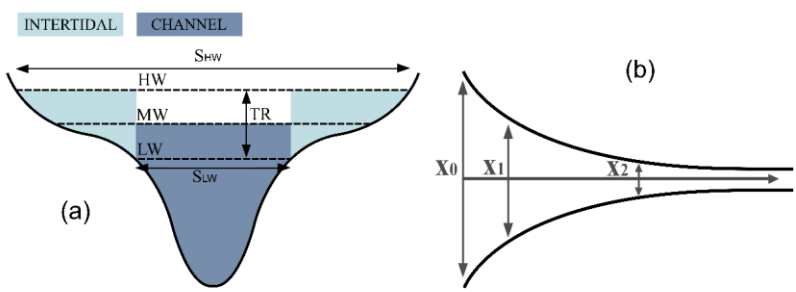

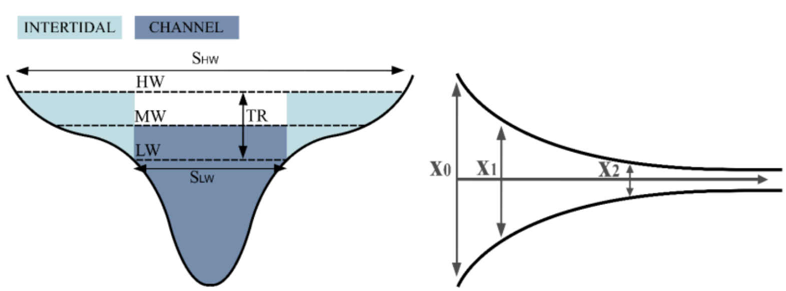

Figure 6: a) S~~s~~chematic cross-section with channel and intertidal volume, high water (*HW*), mean water level (*MW*) and low water (*LW*), tidal range (*TR*) and surface area at *HW* and *LW* (S_{HW} and S_{LW}); b) schematic plan view of a funnel~~-~~shaped estuary.

Formatiert: Schriftart: Nicht Kursiv

Formatiert: Schriftart: Nicht Kursiv

3 Results

3.1 Tidal r~~R~~ange along the e~~E~~stuary

In Figure 7, tidal range (*TR)* is visualised for the different simulated scenarios along the profile of the estuary. Other parameters of the vertical tide (high water (*HW)*, low water *(LW)*, mean water *(MW)*) can be found in the appendix A (Figure A1). We focus on the results of the scenarios with 110 cm *SLR* to gain a better system understanding. The results of the scenarios with *SLR* of 55 cm are not shown here in detail, but are included to determine whether the changes due to *SLR* are in principle similar for a different *SLR* scenario. ~~Hereinafter we focus on the results of the scenarios with 110 cm *SLR* to gain a better system understanding. The scenarios with *SLR* of 55 cm are not visualised and analysed in detail.~~ As apparent in Figure 7, the mean tidal range (*TR*) in the Elbe estuary increases in upstream direction to reach~~, reaches~~ a maximum in the Hamburg section and decrease~~s~~ subsequently. The simulation result for the scenario with *SLR*~~sea level rise~~ of 110 ~~-~~cm (~~*slr110t0*~~*slr110*) reveals an increased tidal range (*TR*) due to lower~~decreased~~ *LW* and higher~~increased~~ *HW* relative to the applied *SLR*~~sea level rise~~ of

Formatiert: Schriftart: Kursiv

Formatiert: Schriftart: Kursiv

Formatiert: Schriftart: Kursiv

Formatiert: Schriftart: Kursiv

Formatiert: Schriftart: Kursiv

Formatiert: Schriftart: Kursiv

110 -cm. *TR* is increased by up to around 15 -cm in the mouth section and by around 10 -cm in the lower section. Upstream of the Hamburg section~~,~~ the increase ~~of *TR*~~ intensifies, mainly due to a lower~~ed~~ *LW*. ~~-~~If~~In the case that~~ tidal flats are elevated by 50 % with *SLR* (*slr110tf55a*), no notable changes in *TR* are visible compared to scenario ~~*slr110t0*~~*slr110*. If, however, tidal flats in the German Bight and the mouth section of the estuary are fully (100 %) elevated with *SLR*~~sea level rise~~ (*slr110tf110a*), *TR* is damped relative to scenario ~~*slr110t0*~~*slr110*. In contrast~~ry~~, an additional elevation of the tidal flats in the entire Elbe estuary (~~*slr110t110e*~~*slr110tf110b*) strongly increases *TR* relative to scenario ~~*slr110t0*~~*slr110*, especially in the lower section.

Formatiert: Schriftart: Kursiv

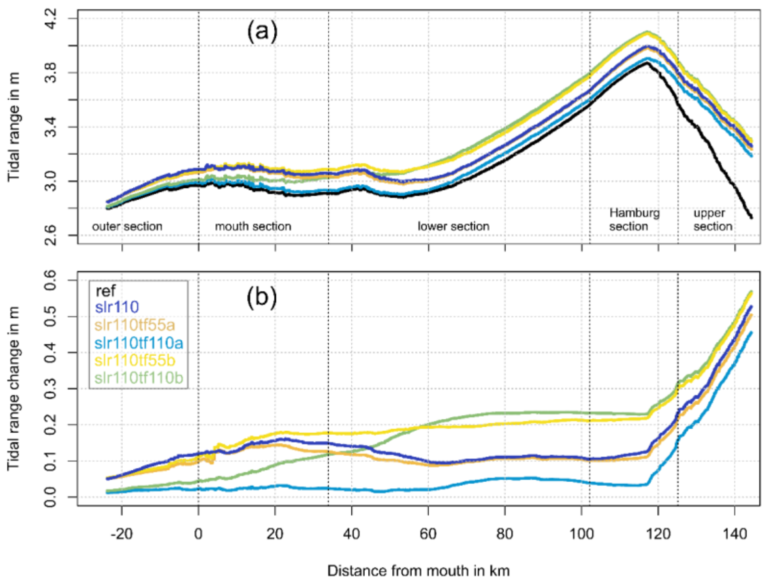
(a)
Tidal range in m
4.2
3.8
3.4
3.0
2.6
outer section
mouth section
lower section
Hamburg section
upper section
(b)
ref
slr110
slr110tf55a
slr110tf110a
slr110tf55b
slr110tf110b
Tidal range change in m
0.6
0.5
0.4
0.3
0.2
0.1
0.0
-20
0
20
40
60
80
100
120
140
Distance from mouth in km

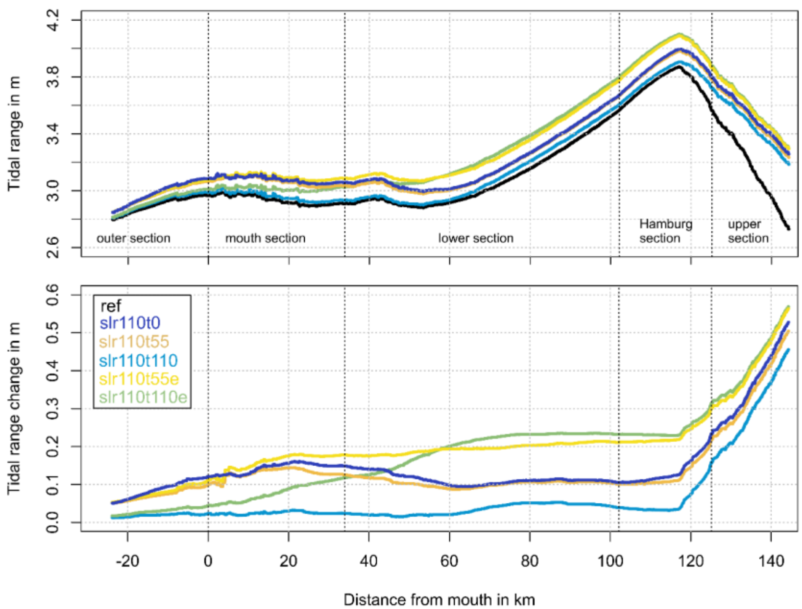

Figure 7: *TR* in m (top) and change in *TR* relative to reference condition in m (bottom) along the estuary profile analysed for a spring~~–~~-neap cycle for scenarios *ref* (black), ~~*slr110t0*~~ *slr110* (dark blue), ~~*slr110t55*~~ *slr110tf55a* (orange), ~~*slr110t110*~~ *slr110tf110a* (light blue), ~~*slr110t55e*~~ *slr110tf55b* (yellow), ~~*slr110t110e*~~ *slr110tf110b* (green).

For all scenarios, the maximum value of *TR* along the estuary is reached in the Hamburg section. Table 3~~Table 2~~ lists the changes in maximum~~.~~ *TR* relative to the reference condition (maximum~~.~~ *TR* = 3.87 m) for all simulated scenarios with *SLR* 110 cm as well as *SLR* 55 cm. Maximum *TR* increases by 6.5 cm for an *SLR* of 55 cm and by 12.5 cm for an *SLR* of 110 cm, which is about 11–12 % of the respective *SLR*. Both *SLR* scenarios with 100 % tidal flat elevation in Scenario A (*slr55tf55a* and *slr110tf110a*) show an increase in maximum *TR* that is less than with *SLR* alone. In both *SLR* scenarios with 100 % tidal flat elevation in Scenario B (*slr55tf55b* and *slr110tf110b*) the increase in maximum *TR* is greater than in the scenarios without tidal flat elevation.~~.~~

Formatiert: Schriftart: Kursiv
Formatiert: Schriftart: Kursiv
Formatiert: Schriftart: Kursiv
Formatiert: Schriftart: Kursiv
Formatiert: Schriftart: Kursiv
Formatiert: Schriftart: Kursiv
Formatiert: Schriftart: Kursiv
Formatiert: Schriftart: Kursiv
Formatiert: Schriftart: Kursiv
Formatiert: Schriftart: Kursiv
Formatiert: Schriftart: Kursiv
Formatiert: Schriftart: Kursiv
Formatiert: Schriftart: Kursiv
Formatiert: Schriftart: Kursiv
Formatiert: Schriftart: Kursiv

Table 3~~2~~: Change in maximum~~.~~ TR relative to reference condition

Scenario	*SLR*	Tidal flat elevation	Change in maximum~~.~~ *TR*	Change in maximum~~.~~ *TR* relative to *SLR*
~~*slr55t0*~~*slr55 – ref*	+55 cm	-	+ 6.5 cm	11.9 %
slr55tf55a – ref	+55 cm	+55 cm S~~s~~cenario A	+ 4.5 cm	8.1 %
slr55tf55b~~e~~ – ref	+55 cm	+55 cm S~~s~~cenario B	+ 14 cm	25.5 %
~~*slr110t0*~~*slr110 – ref*	+110 cm	-	+ 12.5 cm	11.4 %
~~*Slr110t55*~~*Slr110tf55a – ref*	+110 cm	+55 cm S~~s~~cenario A	+ 11.1 cm	10.1 %
~~*slr110t110*~~*slr110tf110a – ref*	+110 cm	+110 cm S~~s~~cenario A	+ 3.5 cm	3.2 %
~~*Slr110t55e*~~*Slr110tf55b – ref*	+110 cm	+55 cm S~~s~~cenario B	+ 21.8 cm	19.8 %
~~*slr110t110e*~~*slr110tf110b – ref*	+110 cm	+110 cm S~~s~~cenario B	+ 23 cm	20.9%

~~The analysis shows changes of *TR* in the estuary which strongly differ between the different simulated scenarios. In some tidal flat growth scenarios *TR* is increased relative to sole *SLR* without topographic changes, while in other scenarios it is decreased. At first glance and without further investigation, a simple explanation for these changes is not apparent. To derive explanatory approaches for the changes of *TR*, changes of estuarine geometry for some scenarios are analysed and displayed hereinafter.~~

3.2 Changes of estuarine g~~G~~eometry

~~6~~3.2.1 Convergence l~~L~~ength of cross-sectional ~~-~~flow ~~-~~a~~A~~rea

Figure 8 shows the mean cross-sectional flow area (*A*) at the control-volume boundaries along the estuary. For better readability, the results of the scenarios ~~*slr110t55*~~ *slr110tf55a* and ~~*slr110t55e*~~ *slr110tf55b* are not shown~~ in the figure~~. The depicted~~displayed~~ flow area is the mean area through which the tidal water flux ~~of a tide~~ flows, averaged over one spring~~-~~ neap ~~-~~cycle. The results show a typical upstream decrease in~~of~~ *A* in all scenarios. As a result~~consequence~~ of *SLR*~~sea level rise~~ (scenario ~~*slr110t0*~~*slr110*), *A* increases along the estuary relative to the reference scenario. Elevated tidal flats in the mouth of the estuary (~~*slr110t110*~~ *slr110tf110a* and *slr110tf55a*) cause ~~a decrease of~~ *A* to decrease in this section compared to ~~*slr110t0*~~*slr110*. Additional elevated flats in the lower section of the Elbe estuary (~~*slr110t110e*~~ *slr110tf110b* and ~~*slr110t55e*~~*slr110tf55b*) slightly decrease *A* in this section accordingly.

Formatiert: Schriftart: Kursiv

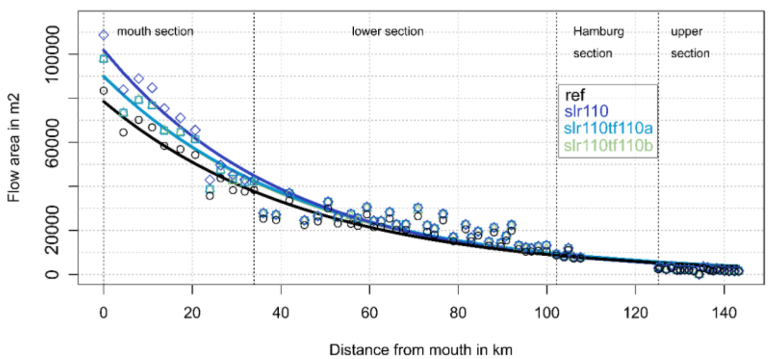

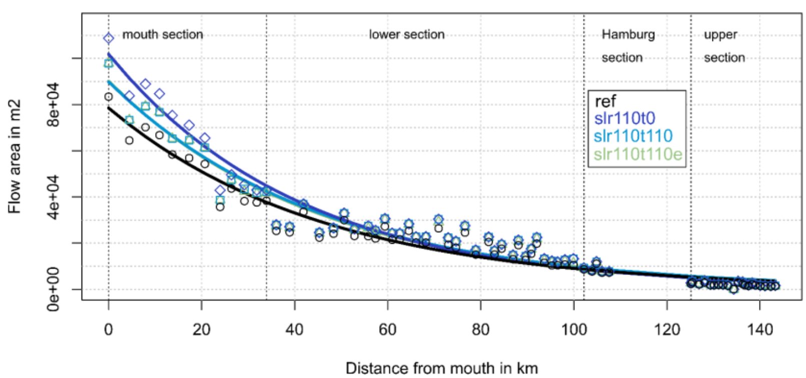

Figure 8: Cross-sectional flow area *A* analysed for each control volume boundary along the estuary profile (markers) and fitted regression model (lines) for the scenarios *ref* (black), ~~*slr110t0*~~ *slr110* (dark blue, rhombuses), ~~*slr110t110*~~ *slr110tf110a* (light blue, squares), ~~*slr110t110e*~~ *slr110tf110b* (green, triangles). (The results of scenarios ~~*slr110t55*~~ *slr110tf55a* and ~~*slr110t55e*~~ *slr110tf55b* are not shown in the figure for better readability.)

The ~~To access the rate at which cross-sectional flow area of an estuary decreases in upstream direction, the~~ geometric parameter of convergence length (L_a) is calculated by fitting an exponential function (Eq. (2)) to the data sets (see 2.3.3). To determine whether~~evaluate, if~~ the convergence length significantly changes between two scenarios, a multiple regression is performed. The results of the weighted multiple non-linear least-~~-~~square regression for all scenarios compared to the reference condition and to ~~all~~ *slr110* ~~scenarios~~ are shown~~displayed~~ in Table 4~~Table 3~~.

Formatiert: Schriftart: Nicht Kursiv

Table 4~~3~~: Results of the multiple non-linear -least-square regression for the cross-sectional -flow -area along the estuary fitted to Eq. (2). Results with a p-value > 0.1 are considered not significant (n.s.).

Scenario	A_0 in m²	p-value of A_0	L_a in km	p-value of L_a
ref	78.5 x10³	<0.001	46.3	<0.001
slr110t0-ref	+23.3 x10³	<0.001	–4.9	0.026
slr110t0	101.7 x10³	<0.001	41.4	<0.001
slr110t110	–11.9 x10³	<0.001	+4.0	0.070
slr110tf110a - slr110t0				
slr110t110e	–11.6 x10³	<0.001	+3.3 (n.s.)	0.130 (n.s.)
slr110tf110b - slr110t0				
slr110t55- slr110t0	–4.8 x10³ (n.s.)	0.134 (n.s.)	+1.3 (n.s.)	0.519 (n.s.)
slr110t55e- slr110t0	–4.6 x10³ (n.s.)	0.148 (n.s.)	+1.0 (n.s.)	0.642 (n.s.)

Scenario	A_0 in m²	p-value of A_0	L_a in km	p-value of L_a
ref	78.5 x 10³	<0.001	46.3	<0.001
slr110 – ref	+23.3 x 10³	<0.001	–4.9	0.026
slr110tf110a – ref	+11.4 x 10³	<0.001	–0.92 (n.s.)	0.690 (n.s.)
slr110tf110b – ref	+11.6 x 10³	<0.001	–1.62 (n.s.)	0.475 (n.s.)
slr110tf55a – ref	+18.5 x 10³	<0.001	–3.56 (n.s.)	0.102 (n.s.)
slr110tf55b – ref	+18.6 x 10³	<0.001	–3.94	0.068
slr110	101.7 x 10³	<0.001	41.4	<0.001
slr110tf110a – slr110	–11.9 x 10³	<0.001	+4.0	0.070
slr110tf110b – slr110	–11.6 x 10³	<0.001	+3.3 (n.s.)	0.130 (n.s.)
slr110tf55a – slr110	–4.8 x 10³ (n.s.)	0.134 (n.s.)	+1.3 (n.s.)	0.519 (n.s.)
slr110tf55b – slr110	–4.6 x 10³ (n.s.)	0.148 (n.s.)	+1.0 (n.s.)	0.642 (n.s.)

The derived convergence length (L_a) of the Elbe estuary for the mean cross-sectional -flow area (A) of the spring- -neap -cycle is 46.3 -km in the reference condition and 41.4 -km in the scenario *slr110t0slr110*. Depending on the p-value for the difference of L_a between two scenarios, the null hypothesis of no change in convergence length L_a can, or cannot be rejected. For the difference between L_a of scenario *slr110t0* and the reference condition, the null hypothesis can be rejected with a significance level of α=005. The detected significant decrease of L_a indicates a stronger convergence, hence a stronger rate of decrease of A in upstream direction due to *SLR* of 110 cm. For the difference of convergence length between scenario *slr110t110* and *slr110t0* the null hypothesis can be rejected with a significance level of α=0.1, which indicates, that in scenario *slr110t110*, convergence is significantly weakened compared to scenario *slr110t0*. For the other scenarios no significant change of convergence length relative to scenario *slr110t0* can be detected with the applied method and a significance level of α≤0.1.

Formatiert: Englisch (Vereinigtes Königreich)
Formatiert: Englisch (Vereinigtes Königreich)
Formatiert: Englisch (Vereinigtes Königreich)
Formatiert: Englisch (Vereinigtes Königreich)
Formatiert: Englisch (Vereinigtes Königreich)
Formatiert: Englisch (Vereinigtes Königreich)
Formatiert: Englisch (Vereinigtes Königreich)
Formatiert: Englisch (Vereinigtes Königreich)
Formatiert: Englisch (Vereinigtes Königreich)
Formatiert: Englisch (Vereinigtes Königreich)
Formatiert: Englisch (Vereinigtes Königreich)
Formatiert: Englisch (Vereinigtes Königreich)
Formatiert: Englisch (Vereinigtes Königreich)
Formatiert: Englisch (Vereinigtes Königreich)
Formatiert: Englisch (Vereinigtes Königreich)
Formatiert: Englisch (Vereinigtes Königreich)
Formatiert: Englisch (Vereinigtes Königreich)
Formatiert: Englisch (Vereinigtes Königreich)
Formatiert: Englisch (Vereinigtes Königreich)
Formatiert: Englisch (Vereinigtes Königreich)
Formatiert: Englisch (Vereinigtes Königreich)
Formatiert: Schriftart: Nicht Kursiv
Formatiert: Schriftart: Nicht Kursiv
Formatiert: Schriftart: Nicht Kursiv
Formatiert: Schriftart: Nicht Kursiv
Formatiert: Schriftart: Nicht Kursiv
Formatiert: Schriftart: Nicht Kursiv
Formatiert: Schriftart: Nicht Kursiv

~~These results are marked with *n.s.* (not significant).~~We decided to consider a significance level of α=0.1. For the difference between L_a of the scenarios *slr110* and *ref*, the null hypothesis can be rejected. The detected significant decrease in L_a indicates a stronger convergence, hence a stronger rate of decrease in A in upstream direction due to *SLR* of 110 cm. The results further show that in scenario *slr110tf110a* convergence is significantly weakened compared to scenario *slr110*, and not significantly different compared to the reference scenario. For the difference between the scenarios *slr110tf55a* and *ref* , we detect a significant decrease in L_a and hence a stronger convergence. For the scenarios *slr110tf55a* and *slr110tf110b* , we cannot detect a significant change in L_a relative to the reference scenario or to *slr110*. However, the results for L_a and their p-values (0.102 and 0.13) indicate that L_a for scenario *slr110tf110b* is larger than for *slr110* and very similar to the reference condition, while L_a for *slr110tf55a* is similar to *slr110*.

3.2.2 Mean hydraulic d~~D~~epth

As mentioned in 2.3.4, the mean hydraulic depth for each section and for each scenario is calculated in two different ways, i.e. including (h_t) and excluding (h_c) intertidal area in~~to~~ the calculation of hydraulic depth. The resulting~~s of~~ mean hydraulic depth values for the reference condition and each *slr110* scenario and section are shown~~displayed~~ in ~~Table 4~~Table 5. Figure 9 illustrates~~displays~~ the relative change in~~of~~ mean hydraulic depth of the scenarios ~~*slr110t0*~~*slr110*, ~~*slr110t110*~~ *slr110tf110a* and ~~*slr110t110e*~~ *slr110tf110b* relative to the reference scenario (*ref*) for each control volume and section.

Table ~~5~~4: Mean and and standard deviation (*SD*) of hydraulic depth of the entire cross-section (h_t) and of the channel (h_c) in the Elbe estuary in m

Scenario	Mouth section		Lower section		Hamburg section		Upper section		Entire estuary	
	h_t	h_c	h_t	h_c	h_t	h_c	h_t	h_c	h_t	h_c
	mean (SD)		*mean (SD)*		*mean (SD)*		*mean (SD)*		*mean (SD)*	
ref	5.7	8.2	8.8	10.6	9.6	10.4	4.7	5.2	7.0	9.2
	(1.3)	(1.8)	(1.5)	(1.4)	(3.1)	(2.8)	(0.4)	(0.4)	(2.5)	(2.8)
~~***slr110t0***~~ ***slr110***	5.7	7.7	8.7	10.5	10.2	11.0	5.1	5.9	6.9	9.0
	(1.0)	(1.7)	(1.4)	(1.5)	(3.3)	(2.9)	(0.6)	(0.3)	(2.5)	(2.5)
~~***slr110t110***~~ ***slr110tf110a***	6.3	8.7	8.7	10.5	10.2	11.0	5.1	6.0	7.4	9.6
	(1.2)	(1.9)	(1.4)	(1.5)	(3.3)	(2.9)	(0.6)	(0.3)	(2.4)	(2.7)
~~***slr110t110e***~~ ***slr110tf110b***	6.4	8.8	9.6	11.1	10.2	11.0	5.1	6.0	7.7	9.9
	(1.4)	(1.9)	(1.5)	(1.5)	(3.3)	(2.9)	(0.6)	(0.3)	(2.7)	(2.7)
~~***slr110t55***~~ ***slr110tf55a***	6.0	8.3	8.7	10.5	10.2	11.0	5.1	6.0	7.2	9.4
	(1.1)	(1.6)	(1.4)	(1.5)	(3.3)	(2.9)	(0.6)	(0.3)	(2.5)	(2.5)
~~***slr110t55e***~~ ***slr110tf55b***	6.0	8.4	9.1	10.9	10.2	11.0	5.1	6.0	7.3	9.5
	(1.1)	(1.7)	(1.5)	(1.4)	(3.3)	(2.9)	(0.6)	(0.3)	(2.6)	(2.6)

Formatiert: Schriftart: Kursiv
Formatiert: Tiefgestellt
Formatiert: Schriftart: Kursiv
Formatiert: Schriftart: Kursiv
Formatiert: Schriftart: Kursiv
Formatiert: Tiefgestellt
Formatiert: Schriftart: Kursiv
Formatiert: Schriftart: Kursiv
Formatiert: Schriftart: Kursiv
Formatiert: Schriftart: Nicht Kursiv
Formatiert: Schriftart: Kursiv
Formatiert: Schriftart: Kursiv
Formatiert: Tiefgestellt
Formatiert: Schriftart: Kursiv
Formatiert: Tiefgestellt
Formatiert: Schriftart: Kursiv
Formatiert: Tiefgestellt
Formatiert: Schriftart: Kursiv
Formatiert: Tiefgestellt
Formatiert: Schriftart: Kursiv
Formatiert: Tiefgestellt
Formatiert: Schriftart: Nicht Kursiv
Formatiert: Schriftart: Nicht Kursiv

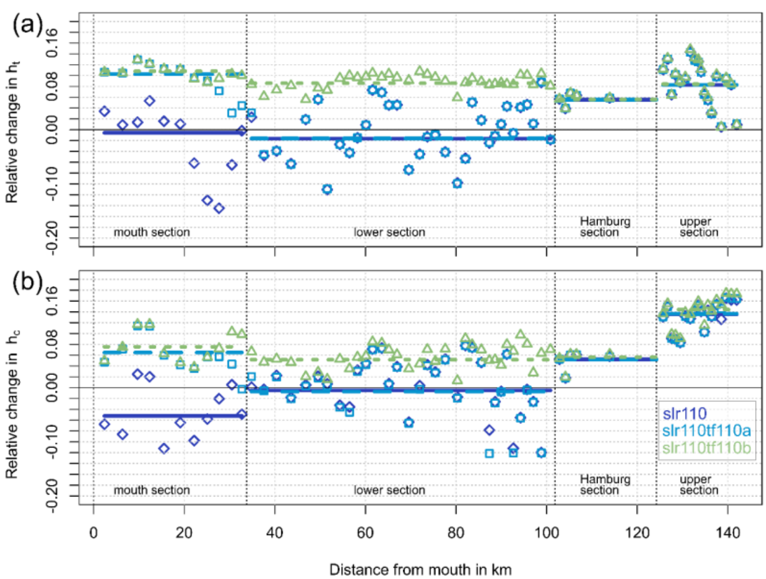

Figure 9: Relative change in~~of~~ mean hydraulic depth (h_t a)~~top~~ and h_c b)~~ottom~~) in each control volume (markers) and each section (lines) relative to reference condition for scenarios ~~*slr110t0*~~ *slr110* (dark blue rhombuses), ~~*slr110t110*~~ *slr110tf110a* (light blue squares), ~~*slr110t110e*~~ *slr110tf110b* (green triangles). (The results of scenarios ~~*slr110t55*~~ *slr110tf55a* and ~~*slr110t55e*~~ *slr110tf55b* are not shown in the figure for better readability.)

The results indicate~~,~~ that *SLR* of 110 cm (~~*slr110t0*~~*slr110*) does not in general cause an increase in mean hydraulic depth along the estuary. As shown in Figure 9, the relative change in h_t and h_c is strongly scattered with an increase in some control volumes and a decrease in others. In the mouth section h_t increases upstream of km 20 and decreases downstream. ~~In contrary, h_t and h_c show even a decrease in some parts of the estuary.~~ Averaged over the sections, ~~*slr110t0*~~ *slr110* has almost no impact on ~~causes almost no changes of~~ h_t in the mouth section and causes it to~~, a slight~~ decrease slightly in the lower section and~~ an~~ increase in the Hamburg section and the upper section. In the scenarios ~~0~~*slr110tf110a* and *slr110tf110b* , mean hydraulic depth clearly increases in the regions where the tidal flats are elevated, and scatter is reduced in these regions. ~~In regions where tidal~~

Formatiert: Schriftart: Nicht Kursiv
Formatiert: Schriftart: Nicht Kursiv
Formatiert: Schriftart: Kursiv
Formatiert: Tiefgestellt
Formatiert: Schriftart: Kursiv
Formatiert: Tiefgestellt
Formatiert: Schriftart: Kursiv
Formatiert: Tiefgestellt
Formatiert: Schriftart: Nicht Kursiv
Formatiert: Schriftart: Kursiv

~~flats are elevated (*slr11t110*: mouth section; *slr110t110e*: mouth section as well as lower section) mean hydraulic depth increases due to *SLR*.~~ The changes in~~of~~ h_c are qualitatively similar to h, exept that mean~~. Mean~~ hydraulic depth excluding intertidal area (h_c) shows a stronger decrease ~~due to~~ solely due to *SLR* ~~and~~ in the mouth section.

3.2.3 Mean r~~R~~elative intertidal a~~A~~rea

The m~~M~~ean relative intertidal area (ϙS_{INT}) in~~for~~ each section along the estuary is shown~~displayed~~ in Table 5 and Figure 10~~Figure 10~~. Figure 10~~Figure 10~~ additionally visualises the relative changes in ϙS_{INT} compared to the reference condition. In general, the relative intertidal area is largest~~greatest~~ in the mouth section and declines~~reases~~ along the estuary towards the Hamburg section.

Table 6~~5~~: Mean and standard deviation (*SD*) of relative intertidal area ϙS_{INT} in the Elbe estuary

~~Scenario~~	~~mouth section~~	~~lower section~~	~~Hamburg section~~	~~upper section~~	~~entire estuary~~
~~*ref*~~	~~0.49~~	~~0.28~~	~~0.16~~	~~0.25~~	~~0.40~~
~~*slr110t0*~~	~~0.41~~	~~0.31~~	~~0.16~~	~~0.34~~	~~0.37~~
~~*slr110t110*~~	~~0.47~~	~~0.31~~	~~0.16~~	~~0.34~~	~~0.39~~
~~*slr110t110e*~~	~~0.47~~	~~0.25~~	~~0.16~~	~~0.35~~	~~0.38~~
~~*slr110t55*~~	~~0.46~~	~~0.31~~	~~0.16~~	~~0.34~~	~~0.39~~
~~*slr110t55e*~~	~~0.46~~	~~0.30~~	~~0.16~~	~~0.34~~	~~0.39~~

Scenario	**Mouth section**	**Lower section**	**Hamburg section**	**Upper section**	**Entire estuary**
	mean (SD)	*mean (SD)*	*mean (SD)*	*mean (SD)*	*mean (SD)*
ref	0.49 (0.07)	0.28 (0.13)	0.16 (0.09)	0.25 (0.10)	0.40 (0.18)
slr110	0.41 (0.07)	0.31 (0.10)	0.16 (0.09)	0.34 (0.12)	0.37 (0.15)
slr110tf110a	0.47 (0.07)	0.31 (0.13)	0.16 (0.09)	0.34 (0.12)	0.39 (0.17)
slr110tf110b	0.47 (0.07)	0.25 (0.13)	0.16 (0.09)	0.35 (0.12)	0.38 (0.17)
slr110tf55a	0.46 (0.07)	0.31 (0.10)	0.16 (0.09)	0.34 (0.12)	0.39 (0.15)
slr110tf55b	0.46 (0.07)	0.30 (0.11)	0.16 (0.09)	0.34 (0.12)	0.39 (0.15)

Formatiert: Schriftart: Nicht Kursiv
Formatiert: Schriftart: Nicht Kursiv
Formatiert: Schriftart: Nicht Kursiv
Formatiert: Absatz-Standardschriftart
Formatiert: Absatz-Standardschriftart
Formatiert: Schriftart: Kursiv
Formatiert: Englisch (Vereinigtes Königreich)
Formatiert: Beschriftung, Abstand Nach: 6 Pt., Nicht vom nächsten Absatz trennen
Formatiert ...
Formatiert: Englisch (Vereinigtes Königreich)
Formatiert ...
Formatiert: Englisch (Vereinigtes Königreich)
Formatiert ...
Formatiert: Englisch (Vereinigtes Königreich)
Formatiert: Englisch (Vereinigtes Königreich)
Formatiert ...
Formatiert ...
Formatiert: Englisch (Vereinigtes Königreich)
Formatiert ...
Formatiert: Englisch (Vereinigtes Königreich)
Formatiert ...
Formatiert ...
Formatiert: Englisch (Vereinigtes Königreich)
Formatiert ...
Formatiert ...
Formatiert: Englisch (Vereinigtes Königreich)
Formatiert ...
Formatiert ...
Formatiert: Englisch (Vereinigtes Königreich)
Formatiert ...
Formatiert ...
Formatiert: Englisch (Vereinigtes Königreich)
Formatiert ...
Formatiert ...
Formatiert: Englisch (Vereinigtes Königreich)
Formatiert ...
Formatiert ...
Formatiert ...

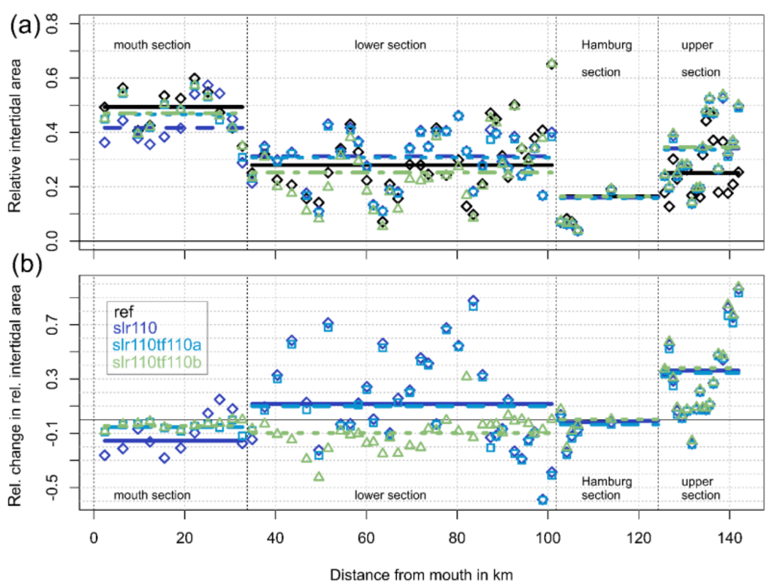

(a)
mouth section
lower section
Hamburg section
upper section
Relative intertidal area
(b)
ref
slr110
slr110tf110a
slr110tf110b
Rel. change in rel. intertidal area
Distance from mouth in km

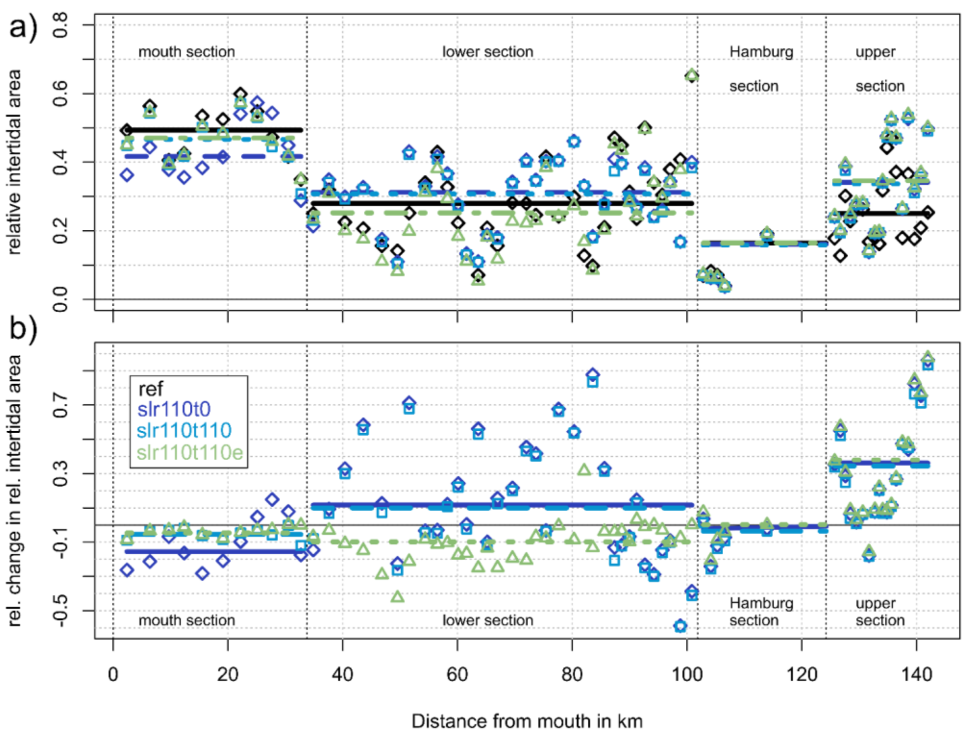

Figure 10: Relative intertidal area (a~~top~~) and relative change in relative intertidal area (b~~ottom~~) in each control volume (markers) and section (lines) along the estuary for scenarios ref (black), ~~*slr110t0*~~ *slr110* (dark blue rhombuses), ~~*slr110t110*~~ *slr110tf110a* (light blue squares), ~~*slr110t110e*~~ *slr110tf110b* (green triangles). (The results of the scenarios ~~*slr110t55*~~ *slr110tf55a* and ~~*slr110t55e*~~ *slr110tf55b* are not shown in the figure for better readability.)

~~Due to *SLR* of 110 cm (*slr110t0*) ϱS_{INT} decreases by about 15% in the mouth section, increases by about 10% in the lower section, remains unchanged in the Hamburg section and strongly increases in the upper section. A tidal flat elevation counteracts the changes of *SLR* in the sections where tidal flats are elevated (mouth section and lower section). In the Hamburg section and the upper section, where no tidal flats are elevated, tidal flat elevation causes almost no changes in ϱS_{INT} relative to *slr110t0*.~~ The relative intertidal area ϱS_{INT} as well as the change in ϱS_{INT} strongly varies between the control volumes along the estuary. Due to *SLR* of 110 cm (*slr110*), ϱS_{INT} becomes smaller in the largest part of the mouth section (downstream of km 25) and mostly increases in the lower (downstream of km 85) and upper sections. Tidal flat elevation counteracts the

Formatiert: Vom nächsten Absatz trennen

Formatiert: Tiefgestellt

Formatiert: Tiefgestellt

Formatiert: Schriftart: Kursiv

Formatiert: Schriftart: Kursiv

Formatiert: Tiefgestellt

changes of *SLR* in the sections where tidal flats are elevated (mouth section and lower section) and results in ρS_{INT} close to the reference scenario for these sections.

4 Discussion

~~4.1 Objectives and Limitations~~

~~Using a three-dimensional hydrodynamic-numerical model of the German Bight, we investigate the effect of potential future *SLR* and tidal flat growth scenarios on tidal dynamics in the Elbe estuary. As it is difficult to predict the future development of tidal flats in the German Bight in the context of accelerated *SLR*, we simulate simplified scenarios with uniformly elevated tidal flats of 0%, 50% and 100% with *SLR*.~~

~~The model calculates water level, current velocity and salt transport on an unstructured orthogonal grid. To reduce computational effort the generation of wind waves as well as sediment and heat transport is not included in our model setup. Thus, potential changes in sediment dynamics, e.g. changes in the *ETM* (estuarine turbidity maximum) and their potential effect on tidal dynamics are neglected. Furthermore, our investigation does not include potential future changes in river discharge into the Elbe estuary, as the discharge in the model is kept constant (600 m³/s).~~

~~However, the aim of this study is to gain a better system understanding of the Elbe estuary in the context of *SLR* and accompanying topographic changes. We do not attempt to produce realistic projections of future changes. Our focus lies on the changes of the vertical tide in the Elbe estuary, especially tidal range *(TR)*, which is closely linked to other tidal parameters and is relevant for several human activities (e.g. navigation, hydraulic structures).~~

~~4.2 Changes in Tidal Range~~

The results show an increase in *TR* in the Elbe estuary because of *SLR*. They also reveal that tidal flat growth with *SLR* can either have no effect, or can decrease or increase *TR* relative to the isolated effect of *SLR*, depending on where and to what extent the tidal flats are elevated. Further analysis shows that the geometric parameters of the Elbe estuary change under the combined impact of *SLR* and tidal flat elevation. In the following section we will discuss the changes in the estuarine geometry and their possible causes. We will then go on to propose explanatory approaches for the changes in *TR* based on changes in geometry.~~Our simulation results show, that *SLR* of 55 and 110 cm causes an increase of *TR* in the estuary as *LW* is elevated less than *HW*. Effects of tidal flat elevation with *SLR* on *TR* strongly differ between the simulated scenarios. Tidal flat elevation can have no effect, decrease or increase *TR* relative to sole *SLR*, depending on the location and amount of tidal flat elevation. Tidal flat elevation in the mouth of the estuary can decrease *TR* while tidal flat elevation in the lower section of the estuary increases *TR* relative to sole *SLR*.~~

~~As a simple explanation for these various changes of *TR* in the different simulated scenarios is not apparent at first glance, changes of estuarine geometry are analysed for reference condition and all scenarios with 110 cm *SLR* to derive explanatory~~

Formatiert: Schriftart: Kursiv
Formatiert: Tiefgestellt

Formatiert: Schriftart: Kursiv
Formatiert: Schriftart: Kursiv
Formatiert: Schriftart: Kursiv
Formatiert: Schriftart: Kursiv
Formatiert: Schriftart: Kursiv
Formatiert: Schriftart: Kursiv
Formatiert: Schriftart: Kursiv

~~approaches. As *TR* shows qualitatively similar changes in the scenarios with *SLR* of 55 cm, those are assumingly induced by similar alterations in estuarine geometry as for a *SLR* of 110 cm. Three geometric parameters were analysed to find indications for the cause of these changes in *TR*: convergence length, mean hydraulic depth and relative intertidal area.~~

~~4.3 Changes in Geometry~~

4.~~3.~~1 Convergence l~~L~~ength

Our estimated value~~s~~ for the estuary's convergence length (L_a) ~~of the estuary~~ in the reference condition is 46.5 km. This value lies in the same order of magnitude as ~~of~~ the values estimated by Dronkers (2017) (42 km) and Savenije et al. (2008) (30 km) for the Elbe estuary. Scenario ~~*slr110t0*~~ *slr110* results in a significant decrease in~~of~~ L_a and therefore a stronger convergence of the Elbe estuary relative to the reference condition. In scenario ~~*slr110t110*~~ *slr110tf110a* ~~a weakening of~~ upstream convergence weakens relative to ~~*slr110t0*~~ *slr110* ~~is detected~~, which results in an L_a close to the reference condition.

A change in L_a is the~~a~~ result of differing ~~stronger or weaker~~ changes in the~~of~~ cross-sectional area (*A*) along the estuary in upstream direction, which are due to regional dissimilarity~~differences~~ in cross-sectional geometry. As discussed in Friedrichs et al. (1990), changes in of intertidal storage capacity, cross-sectional flow area and channel width due to *SLR* are~~is~~ strongly dependent on the gradient of the estuary banks. The ~~Correspondingly, the~~ model results correspondingly show a stronger increase in the cross-sectional flow area in the mouth section of the Elbe estuary where ~~which contains larger~~ tidal flat areas (meaning low topographic gradient) are larger compared to other sections. It can therefore be assumed~~,~~ that the stronger~~increased~~ convergence of *A* as a result of ~~in upstream direction due to~~ *SLR* is due to the decrease in the ~~based on the fact that~~ the amount of relative intertidal area further upstream in ~~the Elbe~~ estuary ~~is declining in upstream direction~~ (Figure 10~~Figure 10~~). This effect is sketched in Figure 11. Tidal flat elevation decreases *A* regionally and seems to significantly counteract *SLR*-induced changes in~~of the~~ convergence ~~this effect~~ in scenario ~~*slr110t110*~~*slr110tf110a*, but not in the other scenarios.

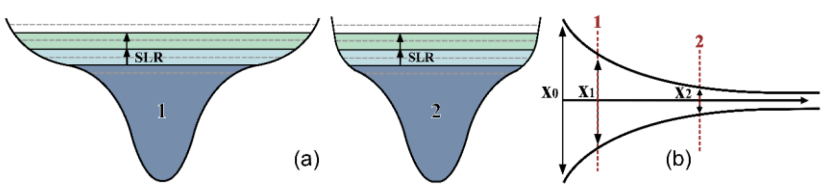

Figure 11: Schematic of SLR in an estuary cross-sections (a) with large (1) and small (2) S_{INT} and schematic plan view of an estuary (b). The black lines in the cross-sections show the MW for a reference scenario (dark blue) and two SLR scenarios (light blue and light green).~~Schematic display of *SLR* in estuary cross-sections (left) and schematic plan view of an estuary (right)~~

Formatiert: Standard

Formatiert: Schriftart: Nicht Kursiv

Feldfunktion geändert

Feldfunktion geändert

Formatiert: Schriftart: Nicht Kursiv

Formatiert: Schriftart: Nicht Kursiv

Formatiert: Schriftart: Nicht Kursiv

Formatiert: Schriftart: Nicht Fett

Formatiert: Schriftart: Nicht Kursiv

Formatiert: Schriftart: Kursiv

4.3.2 Mean hydraulic dDepth

In the reference scenario we derive a mean hydraulic depth averaged over the entire estuary (up tountil the weir in Geesthacht) of 7.0 -m for h_t (including intertidal area) and 9.2 -m for h_c (excluding intertidal area). In comparison, Savenije et al. (2008) listed a mean depth at *MW* of 7.0 -m increasingdecreasing upstream to 9.0 -m further upstream for the Elbe estuary, and Dronkers (2005) listed a time-averaged channel depth of 10.0 -m for the Elbe estuary. However, it is not clear how these numbers were derived.

Our simulation results for the *SLR* scenarios might be unexpected and counter-intuitive since, as they show that *SLR* of 110 -cm does not in general cause an increase in mean hydraulic depth along the estuary. To theIn contrary, the mean hydraulic depth shows varying changes no changes and even a decrease in some parts of the estuary for *slr110t0* *slr110* relative to the reference scenario. These differing changes in mean hydraulic depth along the estuary are caused by the varying topographic gradients ofbetween the control volumes. A decrease inof h_c due to *SLR* can be explained by an effect where the shallow areas next to the previous channels becomeing part of the now enlargedwider channels (Friedrichs et al., 1990): due to an elevated *LW*, some of the areas next to the channel that previously belonged to the intertidal zone can develop into subtidal areas and thus become part of the channel (Figure 12). Because of the relatively small water depth in this new part of the channel, the hydraulic depth averaged over the channel cross-section can decrease. Moreover, elevated *HW* can cause and a the decrease of h_t can be in addition explained by shallow previously supratidal areas to become becoming intertidal areas (see Figure 12), which exlaines the decrease in h_t. However, ifIf tidal flats are elevated with *SLR* in the model, this results inthey cause a regional increase in mean hydraulic depth relative to *slr110t0* *slr110* and relative to the reference condition in the Elbe estuary. This can be explained by tTidal flat elevation counteractsing the previouslyabove–mentioned effect whereof shallow areas becomeing part of the subtidal and intertidal cross-sections and this, which overall results in a greatern increase of mean hydraulic depth due to *SLR* in these scenarios.

4.3.3 Relative intertidal aArea

We define relative intertidal area (ϱS_{INT}) as the ratio between intertidal area and wet surface area at high water (Sect. 2.3.5). For the reference condition we analyse a mean ϱS_{INT} of 0.4 for the entire estuary, which is slightly lower than the value of 0.5 derived by Dronkers (2005) for the Elbe estuary and in the range of 0.412 to 0 (decreasing in upstream direction) to 0 given by Savenije et al. (2008). Note that Dronkers (2005) and Savenije et al. (2008) used a different form (ratio of width at *HW* to width at *LW*) and that these numbers are converted for comparability. According to our simulation results, *SLR* of 110 cm causes regionally strongly widely scattered changes in ϱS_{INT} along the estuary with a decrease in some control volumes and an increase in others. According to our simulation results, *SLR* of 110 cm causes regionally strongly varying changes of ϱS_{INT}, namely a decrease of ϱS_{INT} in the mouth section and an increase in the lower section and the upper section of the estuary. Tidal flat elevation counteracts these changes regionally.

Formatiert: Überschrift 2
Formatiert: Schriftart: Nicht Kursiv
Formatiert: Schriftart: Nicht Kursiv
Formatiert: Schriftart: Nicht Kursiv
Formatiert: Schriftart: Kursiv
Formatiert: Schriftart: Kursiv
Formatiert: Schriftart: Nicht Kursiv
Formatiert: Überschrift 2
Formatiert: Schriftart: Kursiv
Formatiert: Tiefgestellt

The varying changes along the estuary can be explained by the differing topographic gradients. In general, *SLR* ~~Sea level rise~~ can ~~in general~~ either cause an increase or~~,~~ decrease in S_{INT}, or it causes no change ~~-~~at all~~in *S_{INT}*~~, depending on the local topographic gradient above *LW* and a potential change in *TR* (see Figure 12). An increase in S_{INT} can ~~be the~~ result from~~of~~ previously supratidal areas (above old *HW*) becoming part of the S_{INT} due to *SLR*~~sea level rise~~ (Dronkers, 2005) and/or it can be caused by an~~the~~ increased~~ of~~ *TR*. A decrease in~~of~~ S_{INT} can occur in tidal systems that~~which~~ are e.g. contained ~~restricted~~ by dikes or restricted by a strong~~high-~~ gradient topography. In such cases the size of previous ~~which can result in larger previously~~ S_{INT} that becomes~~becoming~~ subtidal area (S_{LW}) can be larger as a result of *SLR* than the size of previously supratidal area that becom~~esing~~ S_{INT} due to *SLR* (Dronkers, 2005) (see Figure 12). However, a decrease in S_{INT} ~~and/or~~ can also be caused by a decrease in~~of~~ *TR*.

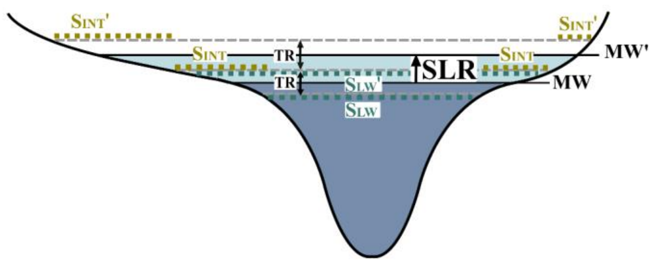

Figure 12: **Schematic of *SLR* in estuary cross-sections and the resulting changes in the intertidal area (S_{INT}) for different topographic gradients between high water (*HW*) and low water (*LW*). The left side of the figure shows a low gradient; the right side shows a higher gradient. The black lines correspond to *MW* for the reference condition (dark blue) and *SLR* (light blue). All parameters with an apostrophe belong to the scenario with *SLR*. The dashed grey lines show *HW* and *LW* for both scenarios; the coloured dotted lines show S_{HW} and S_{LW}.** ~~**schematic display of *SLR* in estuary cross-sections and its resulting change in intertidal area (*S_{INT}*) for different topographic gradients between high water (*HW*) and low water (*LW*)**~~

4.4 ~~Explanatory Approaches for the~~ Changes in t~~T~~idal r~~R~~ange and explanatory approaches ~~based on Changes in Geometry~~

The effects of the previously discussed changes in geometric parameters on tidal dynamics act simultaneously and can therefore counteract, outweigh or enhance each other in the resulting impact~~effect~~ on *TR*. However, we want to point out correlations between the detected changes in~~of~~ geometry and in *TR* to find explanatory approaches for the latter.

SLR of 110 cm without topographic changes

The simulation results show an increased~~ of~~ *TR* in the estuary in scenario ~~*slr110t0*~~ *slr110* relative to the reference condition. The ~~In accordance,~~ analysis of the upstream convergence of the cross-sectional ~~-~~flow ~~-~~area (*A*) accordingly shows a significant increase in~~of~~ convergence in scenario ~~*slr110t0*~~ *slr110* relative to the reference condition. We assume~~suspect~~ this is the main reason for the increased~~ in~~ *TR* in ~~*slr110t0*~~*slr110*, as the gradually convergence~~ing~~ in width and depth causes an amplification

Formatiert: Schriftart: Kursiv
Formatiert: Schriftart: Nicht Kursiv
Formatiert: Schriftart: Nicht Kursiv
Formatiert: Schriftart: Nicht Kursiv
Formatiert: Schriftart: Kursiv
Formatiert: Schriftart: Nicht Kursiv
Formatiert: Schriftart: Nicht Kursiv
Formatiert: Schriftart: Nicht Kursiv
Formatiert: Schriftart: Kursiv
Formatiert: Schriftart: Nicht Kursiv
Formatiert: Schriftart: Nicht Kursiv
Formatiert: Schriftart: Kursiv
Formatiert: Schriftart: Kursiv
Formatiert: Tiefgestellt
Formatiert: Schriftart: Kursiv
Formatiert: Schriftart: Kursiv
Formatiert: Schriftart: Kursiv
Formatiert: Schriftart: Kursiv
Formatiert: Schriftart: Kursiv
Formatiert: Schriftart: Kursiv
Formatiert: Schriftart: Kursiv
Formatiert: Schriftart: Kursiv
Formatiert: Tiefgestellt
Formatiert: Schriftart: Kursiv
Formatiert: Tiefgestellt

of thea tidal wave according to Green's law (1837) (Sect. 2.3.3). Averaged over the different sections, aA decrease inof φS_{INT} is detected in the mouth section and an increase is detected further upstream are detected. Averaged over the entire estuary φS_{INT} decreases. These, which could also contribute to or counteract to the increase in *TR* respectively (Sect. 2.3.5). According to our analysis, *SLR* of 110 cm does not cause a general increase in mean hydraulic depth, but causes strongly varying changes along the estuary. Averaged over the sections, mMean hydraulic depth remainsstays approximately –unchanged relative to the reference condition forin the largest part of the estuary. Overall it slightly decreases, thus potentially counteracts the increase of *TR* (Sect. 2.3.4). In the Hamburg section and the upper section a greater an increase of mean hydraulic depth is detected. The hydrodynamics in this upper part of the estuary are not fully dominated by the tide, but are also highly influenced by the discharge. We Therefore, we assume the strong increase in *TR* in these sections to be caused by an increase inof tidal influence relative to discharge-influence.

SLR of 110 -cm with tidal flat elevation in Sscenario A

In scenario *slr110tf55a*, *TR* is the same as in does not change compared to *slr110t0slr110*. –AccordinglyIn accordance, an analysis of convergence does not shows no significant changes compared to *slr110t0slr110*. The effect of the detected increase of φS_{INT} in the mouth section might be counteracted by the increase of mean hydraulic depth in this section and therefore does not change *TR* relative to *slr110t0*. In contrast, However, if the tidal flats in Sscenario A are elevated by 100 % with *SLR* (*slr110t110slr110tf110a*), *TR* decreases relative to *slr110t0 slr110* along the entire estuary. Our In accordance, our analysis accordingly shows a significant decrease inof convergence forin *slr110t110 slr110tf110a* compared to *slr110t0slr110*, which might be the main reason for *TR* to the decrease in *TR*. On average, the mouth section is characterized by an increase in both relative intertidal area and mean hydraulic depth, the impacts of which might counteract each other. An increase of φS_{INT} and mean hydraulic depth is detected in the mouth section which might contribute and counteract to the decrease of *TR* respectively.

SLR of 110 cm with tidal flat elevation in Sscenario B

In scenario *slr110tf55b*, the tidal flat elevation scenarios B with tidal flat elevation in the German Bight, the mouth section and the lower section of the estuary (*slr110t55e* and *slr110t110e*), *TR* shows a strongly increases relative to *SLR* alone (scenario *slr110t0slr110*) in the entire estuary, while in scenario *slr110tf110b* a decrease can be seen in the mouth section, and an increase is observed further upstream. .In both these scenarios, a significant change in convergence relative to *slr110t0 slr110* cannot be detected with a and significance level of α=0.1. .The aAverage of φS_{INT} in the lower section shows aA decrease for scenario *slr110tf110b* compared to scenario *slr110* in φS_{INT} relative to *slr110t0* is detected in the lower section which might partly explain be part of the reason for the increase inof *TR*. However, a notable decrease in *slr110tf55b* cannot be seen. ThereforeHowever, we assumesuspect that the main reason for the increase in *TR* in these scenarios *slr110tf55b* and *slr110tf110b* the main reason for the increase in *TR* is due to the change in mean hydraulic depth, which increases as the tidal flats are elevated. In contrast to the scenarios where the tidal flats are only elevated in the mouth of the estuary, -mean hydraulic depth increases in a much larger part of the estuary and is therefore most likely to have a stronger effect on *TR*. Therefore, compared to the reference condition, both convergence and hydraulic depth are increased in these scenarios, with both changes presumably leading to an increase in *TR*. As mentioned in Sect. 2.3.4, changes in water depth influence frictional damping of

Formatiert: Schriftart: Kursiv

Formatiert: Schriftart: Kursiv

Formatiert: Schriftart: Kursiv

Formatiert: Schriftart: Nicht Kursiv

Formatiert: Schriftart: Nicht Kursiv

a tidal wave due to energy dissipation and they can also push a system closer to, or further away from resonance. Whether the increase in *TR* due to increased mean hydraulic depth is mainly caused by a decrease in~~of~~ frictional damping or by a shift towards resonance is a question that needs further investigation.

4.5 Comparison to other studies

Formatiert: Überschrift 2

Seiffert and Hesser (2014) simulated the effects of 80 cm *SLR* without topographic changes in the Elbe estuary and found an increase in *TR*, which is in accordance with our results. Jordan et al. (2021) did n~~’~~ot focus on the estuaries when investigating the effects of *SLR* and tidal flat elevation on tidal dynamics in the Wadden Sea. ~~Anyhow~~Nevertheless, their results show a slight increase in M2 amplitude in the Elbe estuary due to *SLR* of 80 cm without tidal flat elevation. They also show a much stronger increase when the tidal flats are elevated in the entire estuary, which qualitatively corresponds to our results. Du et al. (2018) analysed tidal response to *SLR* in different types of idealised estuaries and for different realistic estuaries in the USA. The authors point out the relevance of length, convergence and lateral bathymetry of estuaries for the resulting changes due to *SLR*. In contrast to our study, they tried to find explanatory approaches for the changes in realistic estuaries by matching their geometric characteristics to the different types of geometry of idealized estuaries (e.g. differences in length, convergence and cross-sectional bathymetric gradient), but did not analyse the changes in geometry due to *SLR*. Without further evaluating, they mention the possible change in convergence characteristics under *SLR* conditions and spatially variable tidal response due to spatially variable lateral geometry (e.g. size of intertidal area).

Formatiert: Schriftart: Kursiv
Formatiert: Schriftart: Kursiv
Formatiert: Schriftart: Kursiv
Formatiert: Schriftart: Kursiv
Formatiert: Schriftart: Kursiv
Formatiert: Schriftart: Kursiv
Formatiert: Schriftart: Kursiv
Formatiert: Schriftart: Kursiv

4.6 Limitations

In our study, *SLR*-induced changes in tidal dynamics seaward of the German Bight model are neglected. Previous research by Jordan et al. (2021) shows large-scale changes in M2 amplitude in the North Sea due to *SLR*. Relating the results of Jordan et al. (2021) to our model boundary, we neglect changes of the M2 amplitude that are less than ±2 cm. We assume that this has no bearing on the key results of our study, which aims to improve system understanding of the changes in the Elbe estuary induced by *SLR* and tidal flat growth.

To reduce computational effort, the generation of wind waves as well as sediment and heat transport is not included in our model setup. Hence, potential changes in sediment dynamics, e.g. changes in the *ETM* (estuarine turbidity maximum) and their potential effect on tidal dynamics are neglected. Furthermore, our investigation does not include potential future changes in river discharge into the Elbe estuary, as the discharge in the model is kept constant (600 m³/s).

We selected the *SLR* scenario of 110 cm with corresponding hypothetical tidal flat elevation scenarios which we analysed in detail. For scenarios with 55 cm *SLR* we found qualitatively similar changes in maximum *TR* and therefore assume similar alterations in estuarine geometry. However, to ensure that our results are in principle applicable to other scenarios than an *SLR* of 110 cm, it would be necessary to simulate a range of several *SLR* scenarios with their corresponding tidal flat growth scenarios and analyse the changes in tidal dynamics and estuarine geometry for each of them.

Formatiert: Schriftart: Kursiv

5 Conclusion and o~~O~~utlook

The aim of this study is to gain a better system understanding of the Elbe estuary in the context of sea level rise (*SLR)* and accompanying topographic changes. Using a three-dimensional ~~-~~hydrodynamic-numerical model of the German Bight we investigate the effect of *SLR* and several simplified tidal flat elevation scenarios on the tidal dynamics in the Elbe estuary. With~~Due to~~ *SLR* of 55 cm and 110 ~~-~~cm, the simulation results reveal an increase in the~~of~~ tidal range (*TR*) in the estuary. ~~The results further show, that potential tidal flat elevation with *SLR* has a notable effect on *TR*, which strongly differs between the scenarios.~~ The results further show, that p~~P~~otential tidal flat growth can either have no effect, or cause a decrease or increase in *TR* relative to the isolated effect of ~~sole~~ *SLR*, depending on the location and extent ~~amount~~ of tidal flat elevation. Further analysis of the simulation results is conducted for the scenarios with 110 ~~-~~cm *SLR*. We analyse three geometric parameters of the estuary to find indications explaining~~for~~ the causes of ~~the~~ changes in *TR*: convergence of cross-sectional-flow area, mean hydraulic depth and relative intertidal area.

The results reveal an increase in~~of~~ upstream convergence of the cross-sectional ~~-~~flow ~~-~~area in the estuary which is solely due to ~~sole~~ *SLR* of 110 ~~-~~cm. This effect~~, which~~ is counteracted in the tidal flat growth scenario ~~*slr110t110*~~*slr110tf110a*~~,~~ where the tidal flats in the mouth of the estuary grow to 100 % with *SLR*. Our analyses suggest that these changes in estuarine convergence might be the main reason for the respective increase and decrease in~~of~~ *TR* in these scenarios. Additionally, we find that ~~sole~~ *SLR* alone does not cause a general increase in~~of~~ mean hydraulic depth along the estuary, but causes~~shows~~ almost no changes or even a decrease in large parts of the estuary. However, if the tidal flats are elevated in combination with *SLR*, mean hydraulic depth ~~is increased~~ in the elevated regions increases~~of the tidal flat elevation~~. Therefore, an ~~additional~~ elevation~~increase~~ of the tidal flats in the entire ~~lower section of the~~ estuary (scenarios ~~*slr110t55e*~~ *slr110tf55b* and ~~*slr110t110e*~~*slr110tf110b*) causes an increase in mean hydraulic depth in a large part of the estuary. This~~, which~~ is probably~~likely~~ ~~to be~~ the main reason for the increase in *TR* in these scenarios relative to ~~sole~~ *SLR* alone~~in these scenarios~~. The results of this study show that the future development of *TR* in the Elbe estuary depends not only on future *SLR* but also on the development of tidal flats. The results further show varying changes in estuarine geometry for the different scenarios, which can explain the differing changes in *TR* and improve understanding of the system in the context of *SLR*.

We are able to use the detected changes in estuarine geometry to find qualitative explanatory approaches for the changes in~~of~~ *TR*. Therefore, the analysis of simplified parameters of estuarine geometry, originally developed in studies with analytical models, has proven useful for understanding and interpreting the results of advanced numerical models. However, to further quantify and separate the influence of the changes in~~of~~ each analysed geometric parameter on *TR*, an analytical model of the estuary could be used with the abovementioned geometric parameters as input values. For further generalised understanding, it would be helpful to conduct similar analyses in other estuaries. We are therefore planning ~~Therefore, in future studies we plan~~ to carry out similar investigations for other estuaries in the German Bight in future studies.

Formatiert: Schriftart: Kursiv

Formatiert: Schriftart: Kursiv

Formatiert: Schriftart: Kursiv

Formatiert: Schriftart: Kursiv

Formatiert: Schriftart: Kursiv

This study focuses on the changes of parameters of the vertical tide, especially *TR* due to *SLR* and potential accompanying tidal flat growth scenarios. Future studies could additionally address the analysis of changes in current velocities, tidal asymmetry and salt intrusion, as they are of concern regarding sediment management and other human activities in and around the estuary as well as biodiversity. This study focuses on the changes occurring in parameters of the vertical tide – especially *TR* – due to *SLR* and potential accompanying tidal flat growth scenarios. Future studies could additionally analyse changes in current velocities, tidal asymmetry, sediment transport and salt intrusion, as they are of concern regarding sediment management and other human activities in and around the estuary as well as for biodiversity.

The In order to mitigate changes caused by future *SLR* the findings of this study are helpful for the development of adaptatation measures in the Elbe estuary. The results underline the importance of taking topographic changes into account when analysing the dependence of tidal dynamics in estuaries on future *SLR*sea level rise, which is necessary, for example, as a basis for adapting infrastructure along the waterway. This study demonstrates that *SLR* and potential corresponding tidal flat elevation scenarios can cause changes in tidal dynamics which are strongly dependent on the individual topography of an estuary and the corresponding change inof estuarine geometry.

Formatiert: Schriftart: Kursiv

Appendix

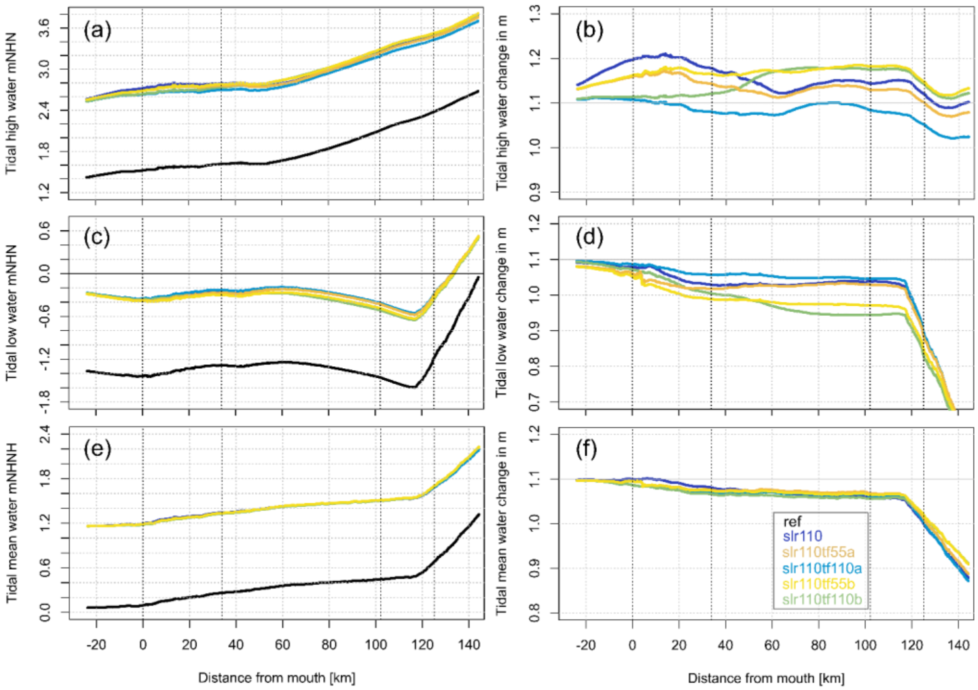

(a)
(b)
(c)
(d)
(e)
(f)
Tidal high water mNHN
Tidal high water change in m
Tidal low water mNHN
Tidal low water change in m
Tidal mean water mNHNH
Tidal mean water change in m
Distance from mouth [km]
Distance from mouth [km]
ref
slr110
slr110tf55a
slr110tf110a
slr110tf55b
slr110tf110b

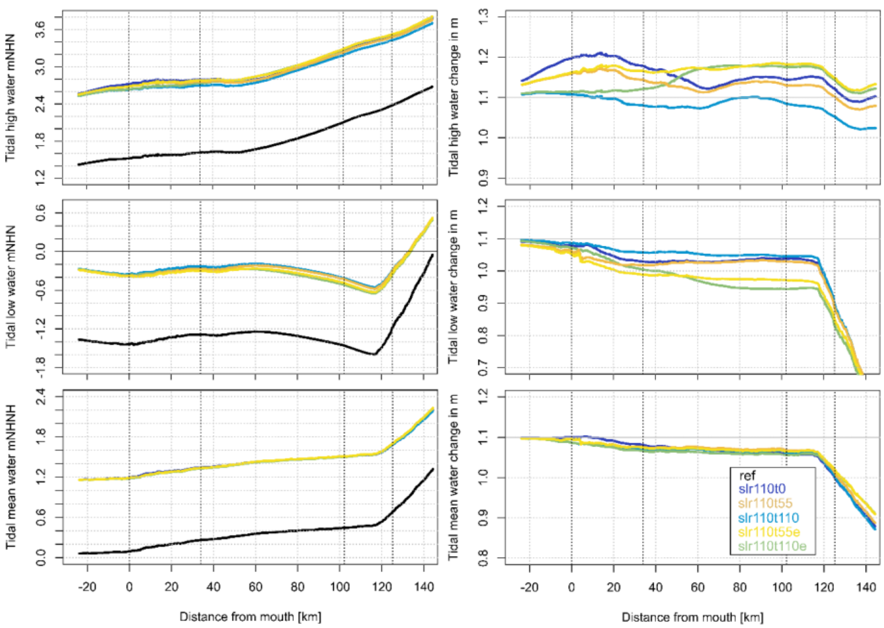

Figure A1: ***HW* (a), *LW* (c) and *MW* (e) relative to mNHN (German vertical d~~D~~atum) ~~(left)~~ and changes in these parameters relative to reference condition in m (b, d and f~~right~~) along the estuary profile analysed for a spring–neap cycle for the scenarios ref (black), ~~*slr110t0*~~ *slr110* (dark blue), ~~*slr110t55*~~ *slr110tf55a* (orange), ~~*slr110t110*~~ *slr110tf110a* (light blue), ~~*slr110t55e*~~ *slr110tf55b* (yellow), ~~*slr110t110e*~~ *slr110tf110b* (green).**

Formatiert: Schriftart: Nicht Kursiv

Formatiert: Schriftart: Nicht Kursiv

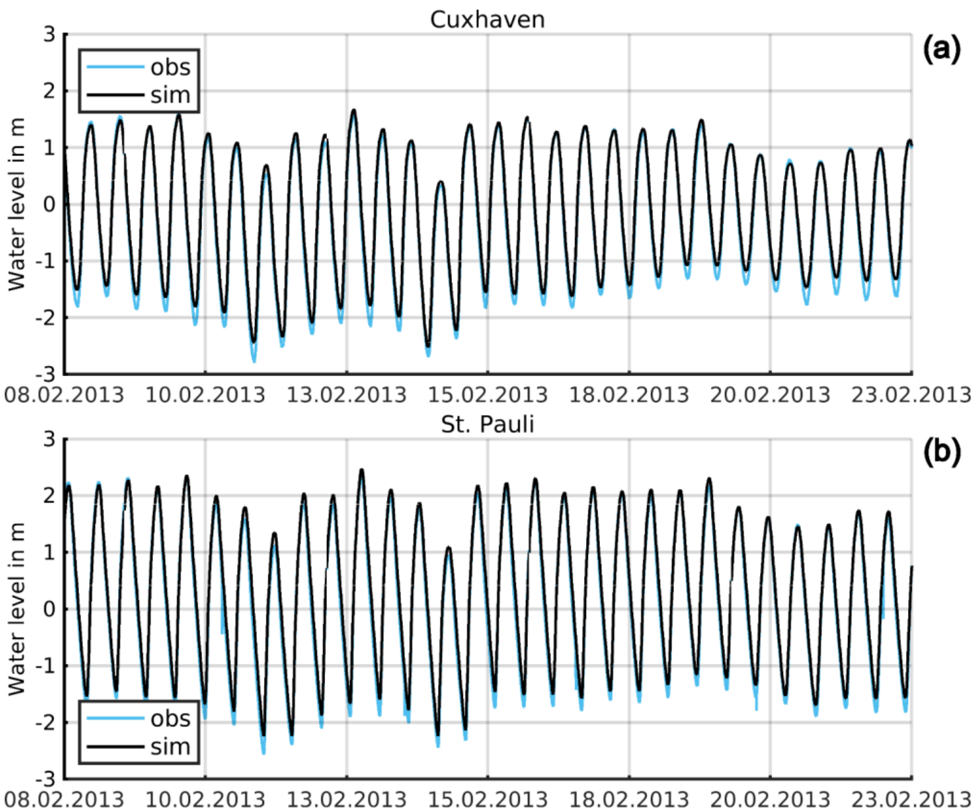

Figure A2: Figure 2: Simulated (black) and observed (blue) water levels at the stations in Cuxhaven (a) and St. Pauli (b)

Data availability

The raw simulation results~~,~~ as well as the results from the analysis are available, ~~up~~on request, from the corresponding author. Water level and river discharge measurement data can be accessed from the open data portal of the Federal Waterways and Shipping Administration (WSV, 2022). The COSMO-REA6 data used for the atmospheric forcing of our model can be accessed from DWD (2022).

Formatiert: Schriftart: Nicht Kursiv

Author contributions

TM worked on the simulations, analysis, figures and interpretation. TM also wrote the article with contributions from RS. JK, PF and RS were involved as scientific experts, supervised the study and gave input for writing and revision of the paper.

Competing interests

The authors declare that they have no conflict of interest.

Acknowledgements

We thank the German Federal Ministry for Digital and Transport for funding this work as part of the Network of Experts. Furthermore, we thank our co-workers at the Federal Waterways Engineering and Research Institute in Hamburg for their continuous support. Special thanks go to Elisabeth Rudolph, Caroline Rasquin, Ingo Hache, Norbert Winkel, Benno Wachler and Ralf Fritzsch for their support and inspiring discussions and to Günther Lang for the development of the employed postprocessing tools. We also thank two anonymous reviewers for their careful reading and valuable suggestions, which led to a substantial improvement of the manuscript.

Funding

This study was funded by the German Federal Ministry for Digital and Transport (BMDV) in the context of the BMDV Network of Experts.

References

Aubrey, D. G. and Speer, P. E.: A study of non-linear tidal propagation in shallow inlet/estuarine systems Part I: Observations, Estuarine, Coastal and Shelf Science, 21, 185–205, doi:10.1016/0272-7714(85)90096-4, 1985.

Baty, F., Ritz, C., Charles, S., Brutsche, M., Flandrois, J.-P., and Delignette-Muller, M.-L.: A Toolbox for Nonlinear Regression in R The Package nlstools, J. Stat. Soft., 66, doi:10.18637/jss.v066.i05, 2015.

BAW: Analysis of calculated results: http://wiki.baw.de/en/index.php/Analysis_of_Calculated_Results, last access: 8 November 2023.

Becherer, J., Hofstede, J., Gräwe, U., Purkiani, K., Schulz, E., and Burchard, H.: The Wadden Sea in transition - consequences of sea level rise, Ocean Dynamics, 68, 131–151, doi:10.1007/s10236-017-1117-5, 2018.

Benninghoff, M. and Winter, C.: Recent morphologic evolution of the German Wadden Sea, Scientific reports, 9, 9293, doi:10.1038/s41598-019-45683-1, 2019.

Bergemann, M.: Salzgehalt am Wehr Geesthacht, personal communication, 2009.

Boehlich, M. J. and Strotmann, T.: Das Elbeästuar, Die Küste 87 (2019), Kuratorium für Forschung im Küsteningenieurwesen (KFKI), doi:10.18171/1.087106, 2019.

Bollmeyer, C., Keller, J. D., Ohlwein, C., Wahl, S., Crewell, S., Friederichs, P., Hense, A., Keune, J., Kneifel, S., Pscheidt, I., Redl, S., and Steinke, S.: Towards a high-resolution regional reanalysis for the European CORDEX domain, Q.J.R. Meteorol. Soc., 141, 1–15, doi:10.1002/qj.2486, 2015.

BSH: Nordseezustand 2008-2011, Bundesamt für Seeschifffahrt und Hydrographie, Hamburg und Rostock, Berichte des BSH, 54, 2016.

Carrère, L., Lyard, F., Cancet, M., Guillot, A., and Roblou, L.: FES 2012: A New Global Tidal Model Taking Advantage of Nearly 20 Years of Altimetry, Noordwijk, ESA SP, 2013.

Casulli, V.: A high-resolution wetting and drying algorithm for free-surface hydrodynamics, Int. J. Numer. Meth. Fluids, 60, 391–408, doi:10.1002/fld.1896, 2009.

Casulli, V. and Walters, R. A.: An unstructured grid, three-dimensional model based on the shallow water equations, Int. J. Numer. Meth. Fluids, 32, 331–348, 2000.

Dissanayake, D. M. P. K.: Modelling morphological response of large tidal inlet systems to sea level rise: Dissertation submitted in fulfillment of the requirements of the Board for Doctorates of Delft University of Technology and of the Academic Board of the UNESCO-IHE Institute for Water Education for the degree of doctor to be defended in public on Monday, 12 December 2011 at 15:00 hours in Delft, the Netherlands, CRC Press, Taylor & Francis Group, Boca Raton, Fla., 1 online resource (viii, 180, 2012.

Dronkers, J.: Dynamics of coastal systems, Advances series on ocean engineering, 25, WORLD SCIENTIFIC, New Jersey, 519 pp., 2005.

Dronkers, J.: Convergence of estuarine channels, Continental Shelf Research, 144, 120–133, doi:10.1016/j.csr.2017.06.012, 2017.

Du, J., Shen, J., Zhang, Y. J., Ye, F., Liu, Z., Wang, Z., Wang, Y. P., Yu, X., Sisson, M., and Wang, H. V.: Tidal Response to Sea-Level Rise in Different Types of Estuaries: The Importance of Length, Bathymetry, and Geometry, Geophys. Res. Lett., 45, 227–235, doi:10.1002/2017GL075963, 2018.

DWD: OPENDATA: https://opendata.dwd.de/climate_environment/REA/COSMO_REA6/, last access: 1 June 2022.

Fox-Kemper, B., Hewitt, H. T., Xiao, C., Aðalgeirsdóttir, G., Drijfhout, S. S., Edwards, T. L., Golledge, N. R., Hemer, M., Kopp, R. E., Krinner, G., Mix, A., Notz, D., Nowicki, S., Nurhati, I. S., Ruiz, L., Sallée, J.-B., Slangen, A., and Yu, Y.: Ocean, Cryosphere and Sea Level Change., In Climate Change 2021: The Physical Science Basis. Contribution of Working Group I to the Sixth Assessment Report of the Intergovernmental Panel on Climate Change, 6, S.1211-1362, doi:10.1017/9781009157896.011., 2021.

Friedrichs, C. T.: Barotropic tides in channelized estuaries, in: Contemporary Issues in Estuarine Physics, Valle-Levinson, A. (Ed.), Cambridge University Press, 27–61, 2010.

Formatiert: Deutsch (Deutschland)

Formatiert: Deutsch (Deutschland)

Friedrichs, C. T.: Tidal Flat Morphodynamics: A Synthesis, Treatise on Estuarine and Coastal Science, 137–170, doi:10.1016/B978-0-12-374711-2.00307-7, 2011.

Friedrichs, C. T. and Aubrey, D. G.: Tidal propagation in strongly convergent channels, J. Geophys. Res., 99, 3321, doi:10.1029/93JC03219, 1994.

Friedrichs, C. T., Aubrey, D. G., and Speer, P. E.: Impacts of Relative Sea-level Rise on Evolution of Shallow Estuaries, in: Residual Currents and Long-term Transport, Cheng, R. T. (Ed.), Springer New York, New York, NY, 105–122, 1990.

Garner, G. G., Hermans, T., Kopp, R. E., Slangen, A. B. A., Edwards, T. L., Levermann, A., Nowikci, S., Palmer, M. D., Smith, C., Fox-Kemper, B., Hewitt, H. T., Xiao, C., Aðalgeirsdóttir, G., Drijfhout, S. S., Golledge, N. R., Hemer, M., Krinner, G., Mix, A., Notz, D., Nowicki, S., Nurhati, I. S., Ruiz, L., Sallée, J.-B., Yu, Y., Hua, L., Palmer, T., and Pearson, B.: IPCC AR6 Sea-Level Rise Projections. Version 20210809.: https://podaac.jpl.nasa.gov/announcements/2021-08-09-Sea-level-projections-from-the-IPCC-6th-Assessment-Report, last access: 16 May 2022.

Garrett, C., Keeley, J. R., and Greenberg, D. A.: Tidal mixing versus thermal stratification in the Bay of Fundy and gulf of Maine, Atmosphere-Ocean, 16, 403–423, doi:10.1080/07055900.1978.9649046, 1978.

Gisen, J.: Prediction in Ungauged Estuaries, 2015.

Green, G.: On the Motion of Waves in a variable Canal of small Depth and Width, Transactions of the Cambridge Philosophical Society, 457–462, 1837.

Holleman, R. C. and Stacey, M. T.: Coupling of Sea Level Rise, Tidal Amplification, and Inundation, Journal of Physical Oceanography, 44, 1439–1455, doi:10.1175/JPO-D-13-0214.1, 2014.

HTG: Empfehlungen des Arbeitsausschusses "Ufereinfassungen" Häfen und Wasserstraßen EAU 2020: (inkl. E-Book als PDF), 12. Auflage, Ernst Wilhelm & Sohn, Berlin, 700 pp., 2020.

Jay, D. A.: Green's law revisited: Tidal long-wave propagation in channels with strong topography, J. Geophys. Res., 96, 20585, doi:10.1029/91JC01633, 1991.

Jordan, C., Visscher, J., and Schlurmann, T.: Projected Responses of Tidal Dynamics in the North Sea to Sea-Level Rise and Morphological Changes in the Wadden Sea, Front. Mar. Sci., 8, 40171, doi:10.3389/fmars.2021.685758, 2021.

Kernkamp, H. W. J., van Dam, A., Stelling, G. S., and Goede, E. D. de: Efficient scheme for the shallow water equations on unstructured grids with application to the Continental Shelf, Ocean Dynamics, 61, 1175–1188, doi:10.1007/s10236-011-0423-6, 2011.

Khojasteh, D., Glamore, W., Heimhuber, V., and Felder, S.: Sea level rise impacts on estuarine dynamics: A review, The Science of the total environment, 780, 146470, doi:10.1016/j.scitotenv.2021.146470, 2021.

Kloepper, S., Baptist, M. J., Bostelmann, A., Busch, J. A., Buschbaum, C., Gutow, L., Janssen, G., Jensen, K., Jørgensen, H. P., de Jong, F., Lüerßen, G., Schwarzer, K., Strempel, R., and Thieltges, D.: Wadden Sea Quality Status Report: https://qsr.waddensea-

Formatiert: Deutsch (Deutschland)

worldheritage.org/?_gl=1*1lhw65f*_ga*MTk4MTkxMDczLjE2OTcwMTU4Njc.*_ga_W7PEFV8FMW*MTY5NzAxNTg2Ni4xLjAuMTY5NzAxNTg2Ni4wLjAuMA., last access: 11 October 1023.

Lang, G.: Analyse von HN-Modell-Ergebnissen im Tidegebiet, Mitteilungsblatt der Bundesanstalt für Wasserbau, 101–108, 2003.

Rasquin, C., Seiffert, R., Wachler, B., and Winkel, N.: The significance of coastal bathymetry representation for modelling the tidal response to mean sea level rise in the German Bight, Ocean Sci., 16, 31–44, doi:10.5194/os-16-31-2020, 2020.

Ray, R. D.: A Global Ocean Tide Model from TOPEX/POSEIDON Altimetry: GOT99.2, NASA, 1999.

S. D. Smith and E. G. Banke: Variantion of the surface drag coefficient with wind speed, Q.J.R. Meteorol. Soc., 101, 656–673, 1975.

Savenije, H. H. G.: Salinity and Tides in Alluvial Estuaries: Second Completely Revised Edition, 2.6th ed., 2012.

Savenije, H. H. G., Toffolon, M., Haas, J., and Veling, E. J. M.: Analytical description of tidal dynamics in convergent estuaries, J. Geophys. Res., 113, doi:10.1029/2007JC004408, 2008.

Sehili, A., Lang, G., and Lippert, C.: High-resolution subgrid models: Background, grid generation, and implementation, Ocean Dynamics, 64, 519–535, doi:10.1007/s10236-014-0693-x, 2014.

Seiffert, R. and Hesser, F.: Investigating Climate Change Impacts and Adaptation Strategies in German Estuaries, Die Küste, 81, 551–563, 2014.

Sievers, J., Malte, R., and Milbradt, P.: EasyGSH-DB: Bathymetrie (1996-2016), 2020.

Simpson, J. H. and Hunter, J. R.: Fronts in the Irish Sea, Nature, 250, 404–406, doi:10.1038/250404a0, 1974.

Song, D., Wang, X. H., Zhu, X., and Bao, X.: Modeling studies of the far-field effects of tidal flat reclamation on tidal dynamics in the East China Seas, Estuarine, Coastal and Shelf Science, 133, 147–160, doi:10.1016/j.ecss.2013.08.023, 2013.

Talke, S. A. and Jay, D. A.: Changing Tides: The Role of Natural and Anthropogenic Factors, Annual review of marine science, 12, 121–151, doi:10.1146/annurev-marine-010419-010727, 2020.

van der Wegen, M.: Numerical modeling of the impact of sea level rise on tidal basin morphodynamics, J. Geophys. Res. Earth Surf., 118, 447–460, doi:10.1002/jgrf.20034, 2013.

van Rijn, L. C.: Analytical and numerical analysis of tides and salinities in estuaries; part I: tidal wave propagation in convergent estuaries, Ocean Dynamics, 61, 1719–1741, doi:10.1007/s10236-011-0453-0, 2011.

Wachler, B., Seiffert, R., Rasquin, C., and Kösters, F.: Tidal response to sea level rise and bathymetric changes in the German Wadden Sea, Ocean Dynamics, 70, 1033–1052, doi:10.1007/s10236-020-01383-3, 2020.

Willmott, C. J., Ackleson, S. G., Davis, R. E., Feddema, J. J., Klink, K. M., Legates, D. R., O'Donnell, J., and Rowe, C. M.: Statistics for the evaluation and comparison of models, J. Geophys. Res., 90, 8995, doi:10.1029/JC090iC05p08995, 1985.

Winterwerp, J. C. and Wang, Z. B.: Man-induced regime shifts in small estuaries—I: theory, Ocean Dynamics, 63, 1279–1292, doi:10.1007/s10236-013-0662-9, 2013.

WSV: Zentrales Datenmanagement (ZDM): Küstendaten: https://www.kuestendaten.de/DE/Services/Messreihen_Dateien_Download/Download_Zeitreihen_node.html.

Zhou, Z., Coco, G., Townend, I., Gong, Z., Wang, Z., and Zhang, C.: On the stability relationships between tidal asymmetry and morphologies of tidal basins and estuaries, Earth Surf. Process. Landforms, 43, 1943–1959, doi:10.1002/esp.4366, 2018.

Zijl, F.: An application of Delft3D Flexible Mesh for operational water-level forecasting on the Northwest European Shelf and North Sea (DCSMv6), Deltares, NGHS Symposium, Delft Software Days, 2014, 2014.

Zijl, F., Sumihar, J., and Verlaan, M.: Application of data assimilation for improved operational water level forecasting on the northwest European shelf and North Sea, Ocean Dynamics, 65, 1699–1716, doi:10.1007/s10236-015-0898-7, 2015.

Zijl, F., Verlaan, M., and Gerritsen, H.: Improved water-level forecasting for the Northwest European Shelf and North Sea through direct modelling of tide, surge and non-linear interaction, Ocean Dynamics, 63, 823–847, doi:10.1007/s10236-013-0624-2, 2013.

Formatiert: Deutsch (Deutschland)